iScience

CellPress
OPEN ACCESS

Article

Hexamethylene amiloride synergizes with venetoclax to induce lysosome-dependent cell death in acute myeloid leukemia

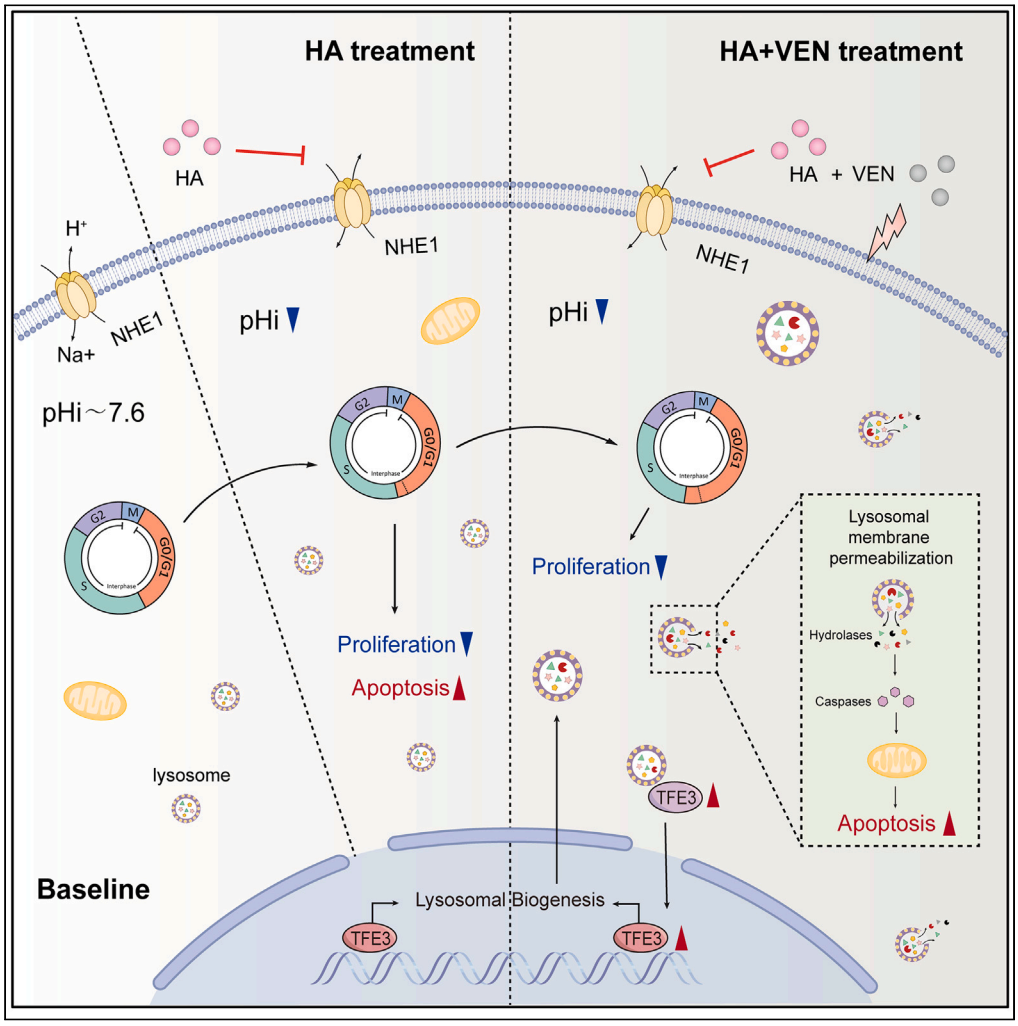

Xinya Jiang, Kexiu Huang, Xiaofan Sun, ..., Rui Huang, Juan Du, Hui Zeng

du.juan@u.nus.edu (J.D.)
androps2011@hotmail.com (H.Z.)

Highlights

High level of NHE1 expression predicts worse prognosis in AML

NHE1 inhibitor HA suppresses AML through arresting cell cycle

HA synergizes with Venetoclax in suppressing AML both *in vitro* and *in vivo*

HA combined with Venetoclax induces lysosome biogenesis and lysosome-dependent cell death

Jiang et al., iScience *27*, 108691
January 19, 2024
https://doi.org/10.1016/j.isci.2023.108691

iScience

CellPress
OPEN ACCESS

Article

Hexamethylene amiloride synergizes with venetoclax to induce lysosome-dependent cell death in acute myeloid leukemia

Xinya Jiang,[1,2,4] Kexiu Huang,[1,4] Xiaofan Sun,[1] Yue Li,[1] Lei Hua,[1] Fangshu Liu,[1] Rui Huang,[3] Juan Du,[1,*] and Hui Zeng[1,5,*]

SUMMARY

Tumors maintain an alkaline intracellular environment to enable rapid growth. The proton exporter NHE1 participates in maintenance of this pH gradient. However, whether targeting NHE1 could inhibit the growth of tumor cells remains unknown. Here, we report that the NHE1 inhibitor Hexamethylene amiloride (HA) efficiently suppresses the growth of AML cell lines. Moreover, HA combined with venetoclax synergized to efficiently inhibit the growth of AML cells. Interestingly, lysosomes are the main contributors to the synergism of HA and venetoclax in inhibiting AML cells. Most importantly, the combination of HA and venetoclax also had prominent anti-leukemia effects in both xenograft models and bone marrow samples from AML patients. In summary, our results provide evidence that the NHE1 inhibitor HA or its combination with venetoclax efficiently inhibits the growth of AML *in vitro* and *in vivo*.

INTRODUCTION

Chemotherapy remains the standard therapeutic approach for acute myeloid leukemia (AML).[1] Although several new drugs have received approval for clinical usage, including the BCL2 inhibitor venetoclax, refractory disease or resistance continues to be a recurring theme,[2,3] and exploring more effective therapies for AML treatment remains necessary.

Intracellular pH dynamics are a vital determinant for cancer progression and chemoresistance.[4,5] Tumors maintain a more alkaline intracellular pH (pHi) dependent on proton exporters, including sodium hydrogen exchangers (NHEs). NHE1 is the first studied member of NHE family,[6,7] and elevated NHE1 expression has emerged as a biomarker for the tumorigenesis and prognosis of solid tumors.[8–10] We previously reported that high NHE1 expression might benefit leukemogenesis.[11] Phenotypically, NHE1 inhibitors have been reported to modulate the cell cycle,[12] induce endoplasmic reticulum stress,[12,13] and regulate autophagy.[14] However, whether targeting NHE1 with inhibitors could inhibit AML cell growth and the underlying mechanisms remain unknown.

Cell death is controlled by signals generated in specific organelles including lysosomes.[15] Lysosomes maintain an acidic pH[16] to ensure the digestive function of hydrolases. These hydrolases could activate apoptotic pathways once released into the cytoplasm, which is defined as lysosomal membrane permeabilization (LMP). Lysosomal alterations endow tumor cells with rapid proliferation ability and drug resistance, making them susceptible to LMP.[17]

Herein, we demonstrate that either NHE1 inhibitor HA alone or combined with venetoclax has satisfactory anti-tumor effects *in vitro* and *in vivo*. Our study provides evidence for a novel therapeutic strategy to enhance the efficacy of chemotherapy in AML.

RESULTS

Inhibition of NHE1 decreases the viability of AML cell lines

Based on our previous finding that NHE1 is the direct target of a tumor suppressive microRNA, we hypothesized that NHE1 might play an oncogenic role in AML. To test this hypothesis, we first analyzed the expression of NHE1 in the TCGA dataset[18] and a large-cohort of AML patients from the Microarray Innovations in Leukemia (MILE) dataset and found that NHE1 is expressed at a higher level in AML patients than normal controls (Figures 1A and S1A). Similarly, another AML cohort from the Gene Expression Omnibus (GSE164894) also demonstrated that NHE1 expression is increased in AML patients who did not achieve complete remission (non-CR) compared to those who achieved CR by '7 + 3' induction (Figure 1B). We next sought to investigate the correlation between NHE1 expression and outcome and

[1]Department of Hematology, The First Affiliated Hospital of Jinan University, Guangzhou, Guangdong 510630, China
[2]Department of Hematology, Xiangya Hospital, Central South University, Changsha, Hunan 410008, China
[3]Department of Hematology, Zhujiang Hospital of Southern Medical University, Guangzhou, P.R. China
[4]These authors contributed equally
[5]Lead contact
*Correspondence: du.juan@u.nus.edu (J.D.), androps2011@hotmail.com (H.Z.)
https://doi.org/10.1016/j.isci.2023.108691

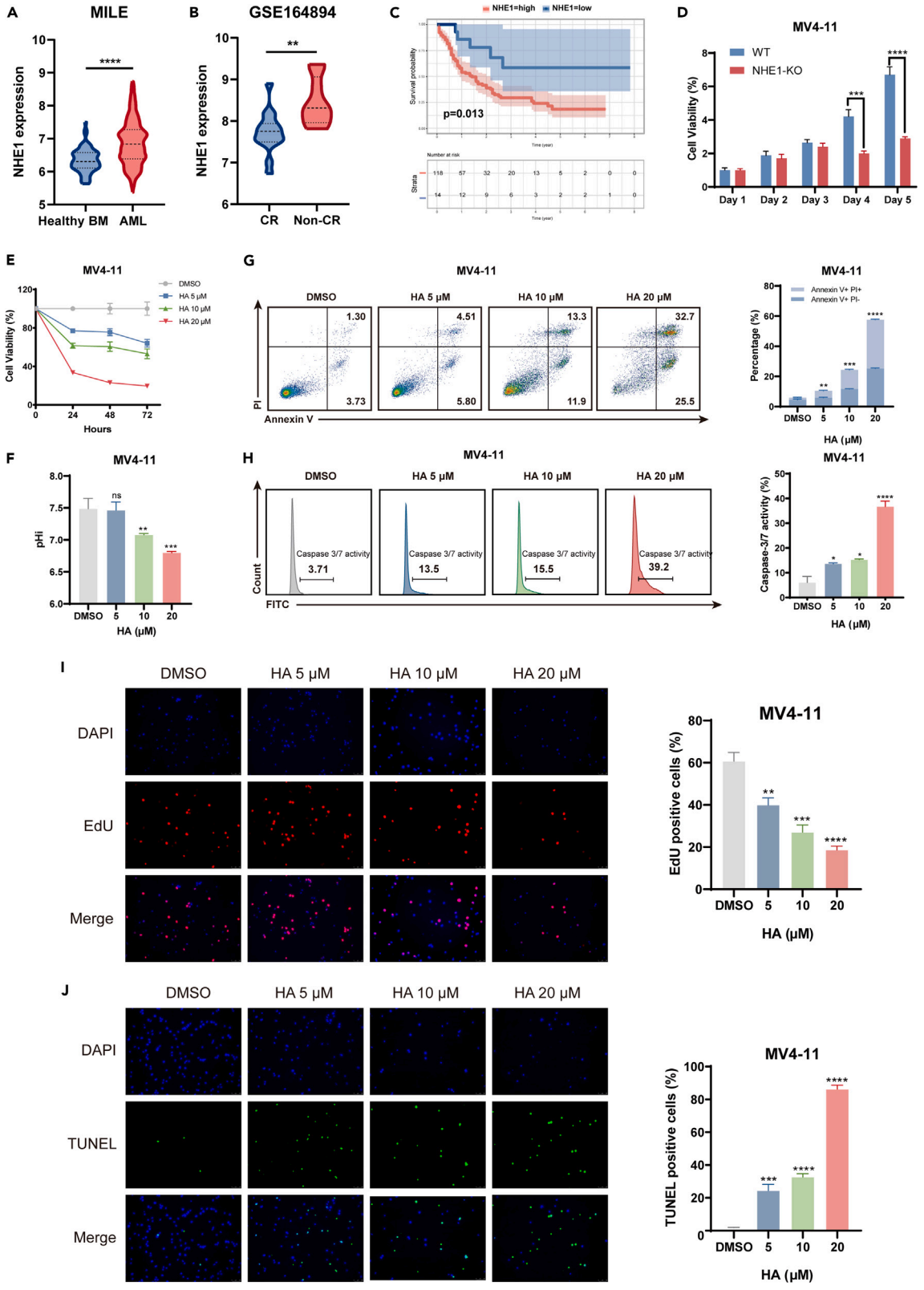
A
MILE
NHE1 expression
****
Healthy BM
AML
B
GSE164894
NHE1 expression
**
CR
Non-CR
C
NHE1=high
NHE1=low
Survival probability
p=0.013
Time (year)
Number at risk
Strata
D
MV4-11
WT
NHE1-KO
Cell Viability (%)
***
****
Day 1
Day 2
Day 3
Day 4
Day 5
E
MV4-11
DMSO
HA 5 μM
HA 10 μM
HA 20 μM
Cell Viability (%)
Hours
G
MV4-11
DMSO
HA 5 μM
HA 10 μM
HA 20 μM
1.30
3.73
4.51
5.80
13.3
11.9
32.7
25.5
PI
Annexin V
MV4-11
Annexin V+ PI+
Annexin V+ PI-
Percentage (%)
HA (μM)
F
MV4-11
pHi
ns
HA (μM)
H
MV4-11
DMSO
HA 5 μM
HA 10 μM
HA 20 μM
Caspase 3/7 activity
3.71
13.5
15.5
39.2
Count
FITC
MV4-11
Caspase-3/7 activity (%)
HA (μM)
I
DMSO
HA 5 μM
HA 10 μM
HA 20 μM
DAPI
EdU
Merge
MV4-11
EdU positive cells (%)
HA (μM)
J
DMSO
HA 5 μM
HA 10 μM
HA 20 μM
DAPI
TUNEL
Merge
MV4-11
TUNEL positive cells (%)
HA (μM)

Figure 1. High NHE1 expression indicates worse prognosis, and NHE1 inhibition with HA reduces the viability of AML cell lines

(A) Comparison of NHE1 expression between primary BMMNCs from AML patients and healthy donors in the MILE dataset.

(B) Comparison of NHE1 expression in primary BMMNCs from AML patients who achieved complete remission (CR) and those who did not achieve CR by "7 + 3" induction in the AML dataset GSE164894.

(C) Overall survival of AML patients from the TCGA database. The patients were divided into low and high groups based on the cut-off value for NHE1 expression.

(D) Effects of NHE1 knockout (KO) on the proliferation of MV4-11. MV4-11 cells were transduced with lentiviruses containing sgRNA targeting NHE1, and they underwent puromycin selection to generate NHE1-KO stable cell lines.

(E) Cell viability dynamics of MV4-11 cells treated with increasing concentrations of HA for 24, 48, and 72 h.

(F) Intracellular pH (pHi) of MV4-11 cells treated with the indicated concentrations of HA for 48 h.

(G–J) MV4-11 cells were treated with increasing concentrations of HA for 48 h. Cells treated with the indicated concentrations of HA were tested by Annexin V/PI staining (G), caspase-3/7 activity (H), EdU assay (I), and TUNEL assay (J). Data are presented as the mean ± SD, and differences were compared using the 2-tailed Student's *t* test. Multiple groups were analyzed with one-way ANOVA. *, $p < 0.05$, **, $p < 0.01$, ***, $p < 0.001$, ****, $p < 0.0001$, ns, not significant.

analyzed the TCGA, MILE, and GEO (GSE12417) datasets using the online web tool GenomicScape. All results demonstrated that patients with higher NHE1 expression exhibit strikingly inferior overall survival (Figures 1C, S1B, and S1C).

To examine the role of NHE1 in AML, we stably knocked down NHE1 using a CRISPR/Cas9 lentivirus-mediated, single-guide RNA system (Figure S1D). As expected, knockdown of NHE1 led to a significant decrease in cell viability (Figures 1D and S1E). Moreover, we also observed a time- and dose-dependent inhibitory effect of NHE1 inhibitor HA on cell viability (Figures 1E and S1F). As NHE1 modulates H^+ extrusion, we next wondered whether HA could affect pHi. After HA administration for 48 h, pHi measurement was conducted by a BCECF-AM probe, and an apparent H^+ accumulation in the HA-treated group was revealed (Figures 1F and S1G). These results are in accordance with the previous studies.[19,20] Moreover, we also observed dose-dependent effects of HA on the promotion of cell death as demonstrated by increased Annexin V^+ cells and caspase-3/7 activity (Figures 1G, 1H, S1H, and S1I). We also observed a dose-dependent decrease in cell proliferation by EdU assay (Figures 1I and S1J), and the accumulation of DNA fragmentation by TUNEL assay (Figures 1J and S1K). Genetic inactivation of NHE1 restrained the effect of HA on cell growth and apoptosis, showing the effect of HA in AML cells is NHE1-dependent (Figures S1L and S1M).

Overall, these observations reveal that NHE1 is preferentially overexpressed in AML, and high levels of NHE1 are correlated with poor prognosis for AML patients. Genetic or pharmacological inhibition of NHE1 effectively reduce cell viability in AML cell lines, indicating that NHE1 might play an important role in the regulation of AML growth.

Cell-cycle arrest is responsible for the growth inhibition induced by HA in AML cells

Considering the anti-leukemia effects of HA, we further sought to explore the underlying mechanisms by RNA sequencing (RNA-seq) analysis. MV4-11 cells incubated with HA (10 μM) or DMSO for 48 h were harvested for transcriptomic analysis to identify their gene expression profiles (Figures 2A and 2B). KEGG pathway enrichment analysis demonstrated significant enrichment for genes involved in "cell cycle" pathways (Figure 2C). Gene ontology (GO) analysis of the down-regulated genes identified categories related to 'regulation of DNA-dependent DNA replication' and 'cell division' (Figure 2D). GSEA also revealed that gene sets associated with the cell cycle were significantly negatively enriched in the HA-treated group (Figure 2E), including CCNB3 and CDKN1A genes (Figure 2F). The expression levels of these cell cycle genes were verified by RT-qPCR (Figure 2G). Consistent with the RNA-seq results, cell cycle analysis using PI staining further demonstrated that treatment with HA dose-dependently arrested the cell cycle in the G0/G1 phase in MV4-11 and MOLM13 cells (Figures 2H and 2I). In summary, these results support the conclusion that HA inhibits AML growth by controlling the cell cycle progression.

HA demonstrates synergistic effects when combined with venetoclax to suppress AML growth *in vitro*

Analysis of TCGA dataset using the "pRRophetic" R package[21] revealed that patients who were insensitive to BCL2 inhibitors exhibited a high NHE1 expression level (Figure S2A). Therefore, NHE1 inhibitors might increase the sensitivity of AML cells to BCL2 inhibitors. To test this hypothesis, we treated AML cells with HA and venetoclax simultaneously. Combined treatment with HA and venetoclax reduced cell viability more effectively than HA or venetoclax alone (Figures 3A and S2B). To further assess the combinatory effects of HA and venetoclax on the proliferation of AML cells, MOLM13 and MV4-11 cells were treated with DMSO, HA (HA group), venetoclax (venetoclax group), or HA plus venetoclax (Combo group) for 48 h. EdU assays demonstrated that the proportion of proliferating cells was dramatically decreased in the Combo group compared to either the HA or venetoclax group (Figures 3B and S2C). In addition to reduction of the proliferation rate, we also observed a prominent additive effect in the Combo group in inducing apoptosis as shown in Annexin V/PI staining and caspase-3/7 activity assays (Figures 3C, 3D, S2D, and S2E). The combination of HA and venetoclax also led to increased DNA fragmentation when compared with either of them as demonstrated by TUNEL assay (Figures 3E and S2F). Of note, although venetoclax did not change pHi, HA plus venetoclax induced a more prominent decrease in pH than HA alone (Figures 3F and S2G).

We next tested whether the combinatory effects of inhibiting AML growth are dose dependent. Our results demonstrated that, at all concentrations tested, the HA and venetoclax combination inhibited growth more efficiently than monotherapy (Figure 3G). To assess whether the combinatory effects are synergistic or additive, we calculated the combination index (CI) using CompuSyn software. The CI value ranged from 0.34 to 0.56 in MV4-11 cells and 0.32 to 0.61 in MOLM13 cells, indicating a medium to strong synergistic antiproliferative effect for treatment with HA and venetoclax (Figures 3H and S2H). Considering both MV4-11 and MOLM13 cell lines harbor FLT3 mutations, we included Kasumi-1, KG-1α and THP-1 cell lines without FLT3 mutation to further test whether the synergy of HA and venetoclax require FLT3 mutation.

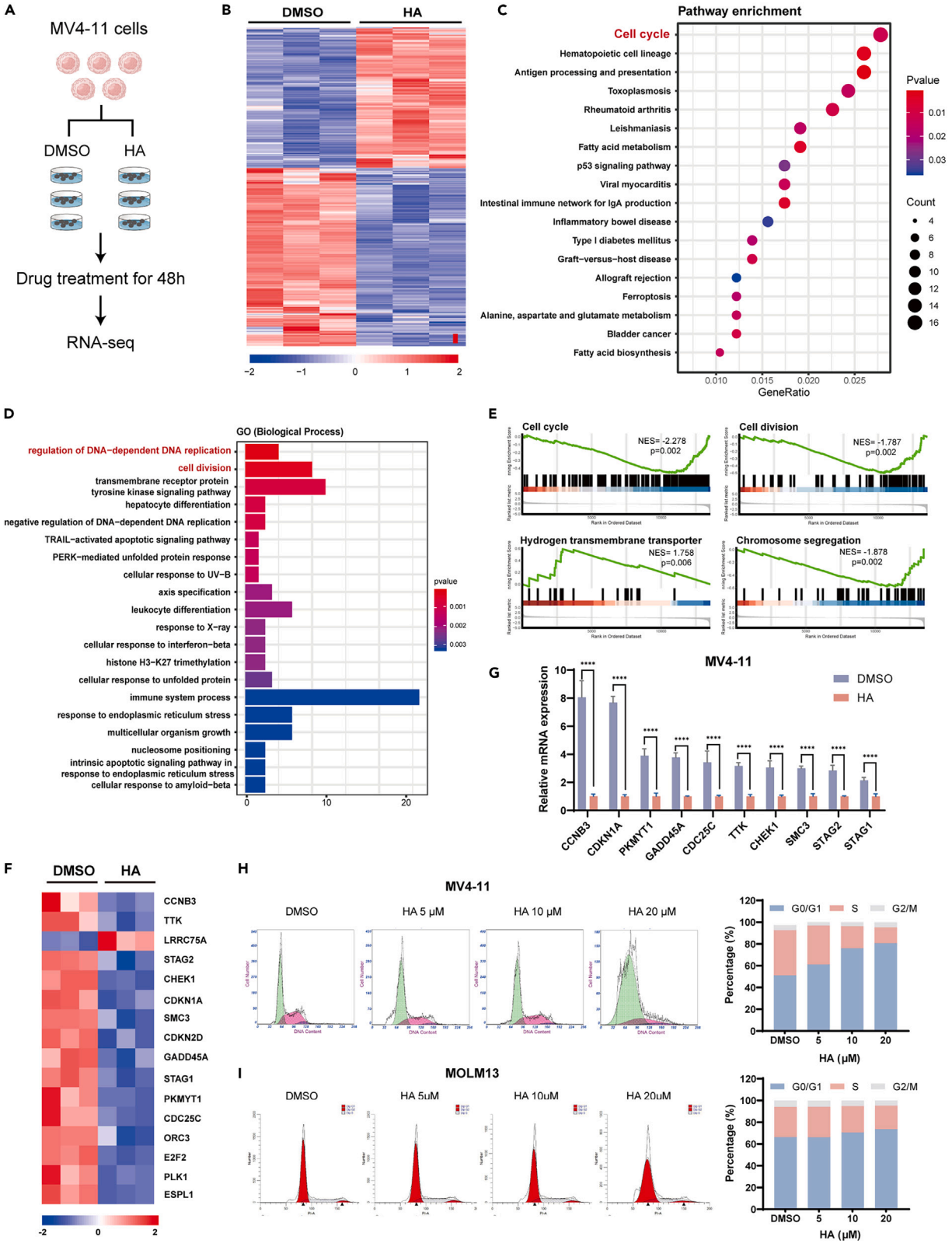
A
MV4-11 cells
DMSO
HA
Drug treatment for 48h
RNA-seq
B
DMSO
HA
−2
−1
0
1
2
C
Pathway enrichment
Cell cycle
Hematopoietic cell lineage
Antigen processing and presentation
Toxoplasmosis
Rheumatoid arthritis
Leishmaniasis
Fatty acid metabolism
p53 signaling pathway
Viral myocarditis
Intestinal immune network for IgA production
Inflammatory bowel disease
Type I diabetes mellitus
Graft−versus−host disease
Allograft rejection
Ferroptosis
Alanine, aspartate and glutamate metabolism
Bladder cancer
Fatty acid biosynthesis
0.010
0.015
0.020
0.025
GeneRatio
Pvalue
0.01
0.02
0.03
Count
4
6
8
10
12
14
16
D
GO (Biological Process)
regulation of DNA−dependent DNA replication
cell division
transmembrane receptor protein tyrosine kinase signaling pathway
hepatocyte differentiation
negative regulation of DNA−dependent DNA replication
TRAIL−activated apoptotic signaling pathway
PERK−mediated unfolded protein response
cellular response to UV−B
axis specification
leukocyte differentiation
response to X−ray
cellular response to interferon−beta
histone H3−K27 trimethylation
cellular response to unfolded protein
immune system process
response to endoplasmic reticulum stress
multicellular organism growth
nucleosome positioning
intrinsic apoptotic signaling pathway in response to endoplasmic reticulum stress
cellular response to amyloid−beta
0
10
20
pvalue
0.001
0.002
0.003
E
Cell cycle
NES= -2.278
p=0.002
Cell division
NES= -1.787
p=0.002
Hydrogen transmembrane transporter
NES= 1.758
p=0.006
Chromosome segregation
NES= -1.878
p=0.002
Rank in Ordered Dataset
G
MV4-11
DMSO
HA
Relative mRNA expression
CCNB3
CDKN1A
PKMYT1
GADD45A
CDC25C
TTK
CHEK1
SMC3
STAG2
STAG1
F
DMSO
HA
CCNB3
TTK
LRRC75A
STAG2
CHEK1
CDKN1A
SMC3
CDKN2D
GADD45A
STAG1
PKMYT1
CDC25C
ORC3
E2F2
PLK1
ESPL1
-2
0
2
H
MV4-11
DMSO
HA 5 μM
HA 10 μM
HA 20 μM
DNA Content
G0/G1
S
G2/M
Percentage (%)
DMSO
5
10
20
HA (μM)
I
MOLM13
DMSO
HA 5uM
HA 10uM
HA 20uM
G0/G1
S
G2/M
Percentage (%)
DMSO
5
10
20
HA (μM)

Figure 2. The cell cycle is responsible for HA-mediated growth inhibition in AML cell lines

(A) Schematic diagram of the experimental design.

(B) Heatmap of gene expression in MV4-11 cells treated with DMSO or HA.

(C) The top enriched pathways by KEGG analysis of MV4-11 cells treated with HA.

(D) GO analysis of the downregulated genes in HA-treated MV4-11cells based on RNA-seq.

(E) Selected GSEA enrichment plots for gene signatures in the HA group.

(F) Heatmap of selected deferentially expressed genes in the cell cycle pathway.

(G) RT-qPCR validation of the genes in panel A in MV4-11 cells.

(H and I) Cell cycle analysis via PI staining. MV4-11 (H) and MOLM13 (I) cells were collected for analysis after the addition of HA for 48 h. Data are presented as the mean ± SD, and differences were compared using the two-tailed Student's *t* test. ****, $p < 0.0001$.

As shown in Figures 3I, 3J, and S2H, potent synergism was confirmed with CI values and further verified with the Bliss model for all cell lines tested, indicating that synergism of HA with venetoclax exists regardless of FLT3 mutation. Collectively, these results illustrate that combining HA with venetoclax exerts synergistic antiproliferative and proapoptotic effects in AML cells.

Lysosomes are mainly responsible for the synergism between HA and venetoclax

To gain insight into the mechanism of how HA and venetoclax synergistically suppress AML cell growth, we performed RNA-seq on MV4-11 cells after treatment with venetoclax plus HA for 48 h (Figure S3A). A total of 3,879 genes were differentially expressed (DEGs) in Combo group compared to the DMSO control group. Among them, 2,722 genes were specifically altered by combined treatment compared to HA or venetoclax treatment alone (Figure S3B). KEGG pathway analysis revealed 'MAPK pathway', 'Lysosome' and 'Cell Cycle' as the top three ranked categories of these 2,722 DEGs (Figure 4A). GSEA analysis also indicated marked activation of lysosome-associated genes and MAPK pathway genes, and suppression of cell cycle-associated genes (Figures 4B and S3C). Consistently, p38 phosphorylation was significantly increased in response to Combo treatment (Figure S3D). Moreover, HA plus venetoclax treatment led to increased G0/G1 phase arrest compared to HA treatment alone as validated by PI staining (Figure S3E). Given that the alterations in cell cycle genes in the Combo group was less significant than differences in apoptosis genes, there may be a novel mechanism accounting for the synergism between HA and venetoclax. Therefore, we hypothesized that lysosomes may be responsible for the combinatory effects. As shown in Figure S4A, the DEGs included LAMP1, CD68, and CTSW, which mainly encode membrane components of lysosomes or hydrolytic enzymes encapsulated by lysosomes. Lysotracker staining confirmed the accumulation of lysosomes in the Combo group (Figures 4C and S4B). Moreover, immunofluorescent imaging and western blotting demonstrated that the expression of LAMP1, which is well recognized as a lysosome marker, is prominently increased at the protein level in the Combo group (Figures 4D and S4C). To better detect morphological changes of lysosome, a transmission electron microscope (TEM) was used and revealed that the lysosomes were elevated in number and volume in the Combo group as compared with the DMSO group (Figures 4E and S4D).

Lysosomal biogenesis is mainly regulated by the microphthalmia/transcription factor E (MiTF/TFE) transcription factors, including TFEB, TFE3 and MiTF.[22] To identify key transcription factor responsible for the lysosome accumulation in the Combo group, we compared the FPKM of these three regulators. The expression level of TFE3 was significantly elevated and showed a 1.3-fold increase at 48 h in the Combo group (Figure 4F). Time-course study revealed that prominent lysosome accumulation became significant from 16 h, so we set 16 h as the time point for further mechanism study (Figure S4E). Increased TFE3 expression was further verified by RT-qPCR and intracellular staining at 16h (Figures 4G and 4H). Notably, TFE3 knockdown could rescue the cytotoxicity effect and abolish lysosomal biogenesis induced by HA + venetoclax (Figures 4I–4K, S4F, and S4G). Therefore, our data suggest that HA plus venetoclax lead to lysosomal biogenesis of AML cells through TFE3.

Considering that lysosomes in cancer cells have weaker membrane stability,[23,24] we sought to evaluate whether the integrity of lysosomal membranes was damaged due to HA plus venetoclax treatment. First, we observed discontinuity in the lysosomal membrane in the Combo group, particularly in larger lysosomes (Figures 4E and S4D), while this alteration was not observed in HA or venetoclax alone group (Figure S4H). Acridine orange (AO) could accumulate in intact lysosomes and emits green fluorescence once it is released from damaged lysosomes, so we used AO staining to examine the membrane integrity of lysosome. As expected, HA plus venetoclax treatment led to increased intensity of green fluorescence, indicating the occurrence of LMP (Figures 4L and S4I). To further confirm the occurrence of LMP, we generated MV4-11 cells that express LGALS3-GFP, which could translocate to leaky lysosomes and is recognized as the best method for LMP detection.[25] HA and venetoclax led to significant LGALS3 puncta formation, similar to the effect of chloroquine (CQ), a well-recognized LMP inducer[26] (Figure 4M). Apart from lysosomal membrane proteins, RNA-seq also revealed upregulation of hydrolases, including cathepsin D (CTSD). We detected an increase in CTSD in the cytoplasm (Figure 4N), and inhibition of CTSD activity with pepstatin A slightly rescued the decease of cell viability resulting from co-treatment with HA and venetoclax (Figure 4O). LMP could induce various forms of programmed cell death (PCD).[27] To identify key pathway of PCD responsible for the effects of Combo in AML, pan-caspase inhibitor Z-VAD-fmk and necroptosis inhibitor Necrostatin-1 were added to AML cells treated with HA and venetoclax. Interestingly, Z-VAD-fmk could rescue the cell viability to a greater extent than Necrostatin-1 (Figure 4P). Consistent with this, combination treatment of HA and venetoclax induced enhanced caspase 3 cleavage (Figure 4Q), demonstrating that apoptosis is the major cell death pathway. In aggregate, our findings suggest that combined treatment with HA and venetoclax induces the accumulation of lysosomes, which undergo increased LMP to facilitate apoptosis of AML cells.

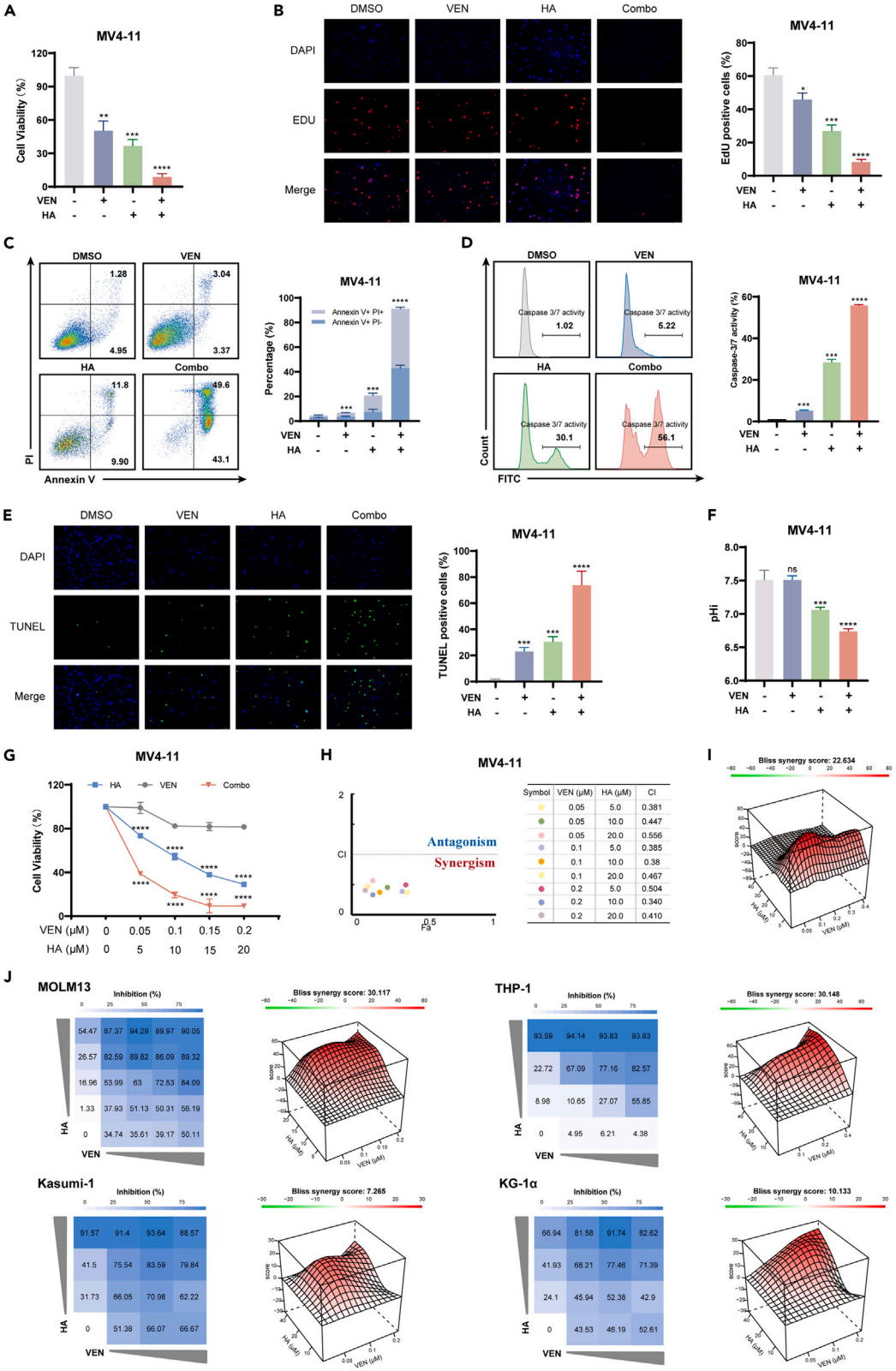
A
MV4-11
Cell Viability (%)
VEN
HA
B
DMSO
VEN
HA
Combo
DAPI
EDU
Merge
MV4-11
EdU positive cells (%)
C
DMSO
VEN
HA
Combo
PI
Annexin V
MV4-11
Annexin V+ PI+
Annexin V+ PI-
Percentage (%)
D
DMSO
VEN
HA
Combo
Caspase 3/7 activity
1.02
5.22
30.1
56.1
Count
FITC
MV4-11
Caspase-3/7 activity (%)
E
DMSO
VEN
HA
Combo
DAPI
TUNEL
Merge
MV4-11
TUNEL positive cells (%)
F
MV4-11
pHi
ns
G
MV4-11
HA
VEN
Combo
Cell Viability (%)
VEN (μM) 0 0.05 0.1 0.15 0.2
HA (μM) 0 5 10 15 20
H
MV4-11
Antagonism
Synergism
CI
Fa
Symbol VEN (μM) HA (μM) CI
0.05 5.0 0.381
0.05 10.0 0.447
0.05 20.0 0.556
0.1 5.0 0.385
0.1 10.0 0.38
0.1 20.0 0.467
0.2 5.0 0.504
0.2 10.0 0.340
0.2 20.0 0.410
I
Bliss synergy score: 22.634
J
MOLM13
Inhibition (%)
54.47 87.37 94.29 89.97 90.05
26.57 82.59 89.82 86.09 89.32
16.96 53.99 63 72.53 84.09
1.33 37.93 51.13 50.31 56.19
0 34.74 35.61 39.17 50.11
Bliss synergy score: 30.117
THP-1
Inhibition (%)
93.59 94.14 93.83 93.83
22.72 67.09 77.16 82.57
8.98 10.65 27.07 55.85
0 4.95 6.21 4.38
Bliss synergy score: 30.148
Kasumi-1
Inhibition (%)
91.57 91.4 93.64 88.57
41.5 75.54 83.59 79.84
31.73 66.05 70.98 62.22
0 51.38 66.07 66.67
Bliss synergy score: 7.265
KG-1α
Inhibition (%)
66.94 81.58 91.74 82.62
41.93 68.21 77.46 71.39
24.1 45.94 52.38 42.9
0 43.53 46.19 52.61
Bliss synergy score: 10.133

Figure 3. HA demonstrates synergistic effects when combined with venetoclax

MV4-11 cells were treated with venetoclax (VEN, 0.1 μM) and HA (10 μM) alone or in combination for 48 h. Treated MV4-11 cells were used in assays assessing cell viability (A), EdU incorporation (B), apoptosis via Annexin V/PI staining (C), caspase-3/7 activity (D), TUNEL analysis (E), and pHi (F).

(G) MV4-11 cells were treated with VEN (0–0.2 μM) either alone or in combination with HA (0–20 μM) for 48 h. Cell viability was measured by CCK8 assay.

(H) Combination Index (CI) for VEN and HA. The CI was calculated by CompuSyn software using MV4-11 cells. CI > 1, CI = 1, and CI < 1 indicate synergistic, additive, and antagonistic effects, respectively.

(I) Cell viability of MV4-11 cells. Cells were treated at the indicated concentrations of VEN (0–0.4 μM) and HA (0–40 μM), and cell viability was determined by the CCK-8 assay following 48 h of treatment. The presence of treatment synergy was determined using the SynergyFinder website, and the Bliss synergy index is denoted as the red regions in the graphs.

(J) Cell viability matrixes and Bliss synergy models of MOLM13, THP-1, Kasumi-1 and KG-1α cell lines. Data are presented as the mean ± SD of at least three independent experiments, and comparisons were evaluated by one-way ANOVA. *, $p < 0.05$, **, $p < 0.01$, ***, $p < 0.001$, ns, not significant.

HA combined with venetoclax reduces the number of AML cells in xenograft models

To further ascertain whether HA monotherapy or the combination of HA and venetoclax is effective in eradicating leukemic cells *in vivo*, we generated a xenograft model using MV4-11-luc$^+$ cells (Figure 5A). Mice were randomly divided into four groups and treated with vehicle, venetoclax (50 mg/kg), HA (20 mg/kg), or venetoclax plus HA (referred to as Combo) for 2 weeks. Mice in the Combo group had dramatically lower bioluminescent signals compared with all other groups (Figure 5B). HA treatment resulted in longer median survival than control, and combined treatment led to more prolonged survival than single agent or control (Figures 5C and 5D). Spleen enlargement was reduced in mice treated with the combination regimen when compared with vehicle control (Figures S5A and S5B). To further examine the tumor burden in the bone marrow (BM), spleen (SP), and peripheral blood (PB), three mice in each group were euthanized after 2 weeks of drug administration. Flow cytometry analysis of human CD45$^+$/CD33$^+$ cells demonstrated a significantly lower AML burden in the bone marrow of mice within the Combo group compared to either inhibitor alone or vehicle control (Figures 5E and 5F). Similarly, reduction of the human CD45$^+$/CD33$^+$ proportion in the PB and SP cells was observed in the Combo group compared to the vehicle or single agent groups (Figures 5G and 5H). IHC analysis of human CD45 cells in the bone marrow and spleen also revealed a reduction in leukemia burden with combination compared to monotherapy (Figure 5I). During with the treatment period, weight loss was not significant in either HA or Combo group (Figures S5C and S5D). Taken together, these results suggest that HA/venetoclax inhibits AML development *in vivo*, which may be an effective and safe alternative therapy for AML treatment.

HA enhances the antileukemic effects of venetoclax in primary AML samples

To further explore the efficacy of HA in treating AML, we collected bone marrow samples from AML patients. Mononuclear cells were cultured with different doses of HA (Figure 6A). The pHi decreased with increasing HA concentrations, implying a significant reduction in proton exportation (Figure 6B). Moreover, HA treatment strongly inhibited viability and dose-dependently induced the apoptosis of primary AML cells (Figures 6C, 6D, and S6A).

Next, we examined whether combination of HA and venetoclax could also decrease the viability of primary AML cells more effectively than either alone. Primary AML cells from 6 patients were treated with each single agent or their combination and were assessed for cell viability. The combination therapy was more efficient than the single agent treatment in most cases (Figure 6E). In addition, as expected, induction of apoptosis was prominently enhanced by combination therapy in AML blast cells (Figures 6F and S6B). Of note, exposure of blast cells to increasing concentrations of HA in combination with venetoclax revealed positive synergistic interactions (Figure 6G). In contrast, slight or no synergism was observed in healthy donors (Figures S6C and S6D), implying the safety of the combination treatment. In summary, HA alone could ameliorate AML, and the combination of HA and venetoclax synergistically eradicates primary AML cells.

DISCUSSION

Dysregulated acid-base balance has been widely implicated in tumorigenesis. For instance, elevation of the intracellular pH destabilizes the R337H domain of p53, leading to loss of its function as a tumor suppressor.[28] Recently, Cheuk Him Man et al. has reported a more alkaline pHi in AML compared to normal hematopoietic stem and progenitor cells *in vivo*.[29] Such a reversed pH gradient is maintained by several proton transporters including NHE1. We found that the NHE1 expression level is elevated in AML patients compared to those who achieve CR, which is in line with the findings by Cheuk Him Man et al.[20] We also found that patients with a high NHE1 expression level had worse overall survival. Genetic or pharmacological inhibition of NHE1 hampers the growth of AML cells, and NHE1 knockdown counteract the effect of HA. Thus, NHE1 inhibitor HA show therapeutic benefit to treat AML, and this effect may be achieved through promotion of intracellular acidification induced by inhibition of NHE1.

Treatment with HA to inhibit tumor growth has been reported in colon carcinoma and triple-negative breast cancer,[30–33] but few studies have explored the mechanism of how HA inhibits tumor growth. HA was reported to alter the structure and function of mitochondria, which leads to the accumulation of ROS in colon carcinoma cells.[33] This drug could can also elicit profound ER stress and paraptosis in breast cancer.[31] In our study, we found that cell-cycle arrest may be a major cause of the toxicity elicited by HA, as HA induced cell-cycle arrest at the G0/G1 phase in a concentration-dependent manner. Moreover, significantly decreased expression levels of cell cycle regulators e.g., CCNB3[34] and CDKN1A,[35] and transcription factors e.g., E2F2,[36] were also observed in HA-treated AML cells. These results are consistent with the cell cycle alterations discovered in gastric cancer[37,38] and leukemia[39] cells in response to HA. Cell cycle progression and DNA synthesis depend

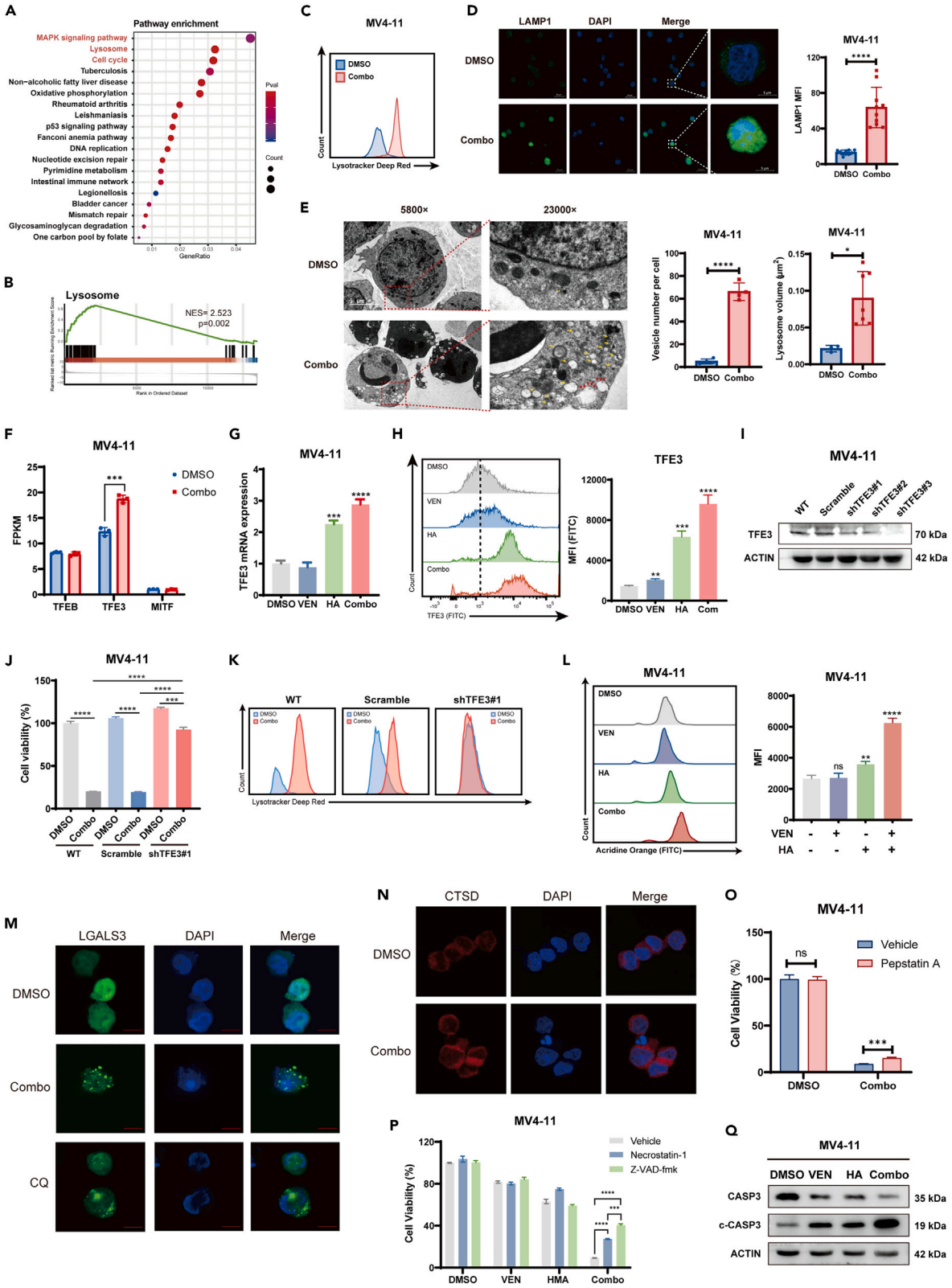
A
Pathway enrichment
MAPK signaling pathway
Lysosome
Cell cycle
Tuberculosis
Non−alcoholic fatty liver disease
Oxidative phosphorylation
Rheumatoid arthritis
Leishmaniasis
p53 signaling pathway
Fanconi anemia pathway
DNA replication
Nucleotide excision repair
Pyrimidine metabolism
Intestinal immune network
Legionellosis
Bladder cancer
Mismatch repair
Glycosaminoglycan degradation
One carbon pool by folate
GeneRatio
Pval
Count
B
Lysosome
NES= 2.523
p=0.002
C
MV4-11
DMSO
Combo
Count
Lysotracker Deep Red
D
LAMP1
DAPI
Merge
DMSO
Combo
MV4-11
LAMP1 MFI
DMSO Combo
E
5800×
23000×
DMSO
Combo
MV4-11
Vesicle number per cell
MV4-11
Lysosome volume (μm²)
DMSO Combo
F
MV4-11
FPKM
DMSO
Combo
TFEB
TFE3
MITF
G
MV4-11
TFE3 mRNA expression
DMSO VEN HA Combo
H
DMSO
VEN
HA
Combo
Count
TFE3 (FITC)
TFE3
MFI (FITC)
DMSO VEN HA Com
I
MV4-11
WT
Scramble
shTFE3#1
shTFE3#2
shTFE3#3
TFE3
70 kDa
ACTIN
42 kDa
J
MV4-11
Cell viability (%)
DMSO
Combo
WT
Scramble
shTFE3#1
K
WT
Scramble
shTFE3#1
DMSO
Combo
Count
Lysotracker Deep Red
L
MV4-11
DMSO
VEN
HA
Combo
Count
Acridine Orange (FITC)
MV4-11
MFI
VEN
HA
M
LGALS3
DAPI
Merge
DMSO
Combo
CQ
N
CTSD
DAPI
Merge
DMSO
Combo
O
MV4-11
Cell Viability (%)
Vehicle
Pepstatin A
ns
DMSO
Combo
P
MV4-11
Cell Viability (%)
Vehicle
Necrostatin-1
Z-VAD-fmk
DMSO
VEN
HMA
Combo
Q
MV4-11
DMSO VEN HA Combo
CASP3
35 kDa
c-CASP3
19 kDa
ACTIN
42 kDa

Figure 4. The major mechanism underlying the synergism of the HA and venetoclax combination involves lysosomal genes

(A) The top 20 enriched pathways identified by KEGG pathway analysis of MV4-11 DMSO-versus-Combo DEGs.

(B) GSEA enrichment plots for lysosome pathways in the Combo group.

(C) Lysotracker staining in the DMSO and Combo groups. MV4-11 cells treated with DMSO or Combo for 48 h were labeled with Lysotracker Deep Red and analyzed by flow cytometry.

(D) Immunofluorescence staining of lysosomes in the DMSO and Combo groups. Fixed MV4-11 cells were stained with an antibody directed against LAMP1 (Green) and DAPI (Blue).

(E) Transmission electron microscope images of MV4-11 cells in the DMSO and Combo groups. scale bar, 1 μm. The yellow arrow indicates lysosomes, and the red arrow indicates lysosomal membrane damage.

(F) FPKM value of TFEB, TFE3, and MiTF in DMSO and Combo group.

(G and H) MV4-11 cells were treated with DMSO, VEN, HA or Combo for 16 h. Cells were harvested to test the TFE3 expression by RT-qPCR (G) and intracellular staining (H).

(I) The knockdown efficiency of TFE3 by western blotting in MV4-11 cells.

(J) Cell viability of the Combo treatment in WT, Scramble and shTFE3 MV4-11 cells.

(K) Lysotracker staining in the DMSO and Combo groups in WT, Scramble and shTFE3 MV4-11 cells.

(L) Flow cytometry analysis of acridine orange-positive MV4-11 cells treated with VEN (0.1 μM) and HA (10 μM) alone or in combination. The MV4-11 cells were stained with acridine orange after treatment for 48 h, and green fluorescence was analyzed by flow cytometry.

(M) Immunofluorescence analysis of LGALS3 localization in the DMSO and Combo groups. MV4-11 cells were transfected with a plasmid encoding LGALS3-GFP, cotreated with VEN and HA, and then analyzed by confocal microscopy. CQ was used as positive control.

(N) Immunofluorescence staining of CTSD in the DMSO and Combo groups.

(O) Cell viability assay of MV4-11 cells cultured with VEN plus HA for 48 h with/without pretreatment with Pepstatin A for 12 h.

(P) Cell viability of MV4-11 cells rescued by Z-VAD-fmk and Necrostatin-1 under the VEN/HA single or Combo treatment.

(Q) Western blotting results of the expression of caspase-3 and cleaved-caspase 3 in MV4-11 cells treated with the indicated drugs. Data are presented as the mean ± SD, and differences were compared using one-way ANOVA. **, $p < 0.01$, ***, $p < 0.001$, ****, $p < 0.0001$, ns, not significant.

largely on alkaline pHi,[40,41] which requires NHE activation to subsequently phosphorylate ribosome S6 protein.[42,43] Intracellular acidification or NHE depletion inhibits G0/G1 progression but not S phase.[44,45] In primary AML cells and leukemic cell lines, a positive correlation exists between pHi and the proportion of S-phase.[39] pHi decrease by MCT4 knockdown reduces proliferation by arresting G1-S transition,[46] which is consistent with the cell cycle alteration in this study after HA administration.

Recent years have witnessed a growing appreciation of the benefit of venetoclax in clinical usage for AML treatment. Nevertheless, venetoclax could still lead to therapeutic resistance.[2,3] One of the underlying mechanisms involves extensive metabolic rewiring. Previous studies by Craig T. Jordan have demonstrated that treatment with the combination of venetoclax and azacitidine inhibits growth in *de novo* AML patients who are selectively reliant on amino acid metabolism.[47] Moreover, Lin et al. mapped the metabolic-apoptotic interactions in AML by treating cells with venetoclax, and they highlighted the oxidative phosphorylation, heme biosynthesis, nucleoside biosynthesis, and glycolysis pathways.[48] However, the role of proton transporters, which control intracellular pH homeostasis, has not been studied in venetoclax-based therapy. Here, we identified and experimentally validated the efficacy of the NHE1 inhibitor HA combined with venetoclax as an efficient combinatory regimen for AML treatment. Intracellular pH assay demonstrated that HA plus venetoclax triggers a more acidic pHi than HA monotherapy. One possible explanation for this phenomenon is the synergistic inhibition of metabolic rewiring. NHE1 induces intracellular alkalization, which subsequently activates catalysis by key metabolic gatekeeper enzymes, including HK1/PKM2/G6PDH, thereby initiating glycolytic flux[29] into AML cells. HA might inhibit this alkalization process and facilitate the metabolic switch from glycolysis to oxidative phosphorylation.[9] Venetoclax could then attenuate oxidative phosphorylation,[49] leading to the unfitness of AML cells. Further studies are needed to elucidate whether the synergism between HA and venetoclax is through pH-dependent metabolism rewiring.

For potential mechanism of synergism between HA and venetoclax, we identified the lysosome pathway as an interesting and important player in AML cells. Increases in lysosome number and volume have been uncovered in AML cells,[17] and these have been implicated in the development of drug resistance as lysosomes can sequester multiple agents.[50,51] However, cancer cells are more susceptible to lysosomal disruption than normal cells, implying that treatments that induce LMP are another avenue worth exploring. In this study, we observed HA and venetoclax led to an increased number of lysosomes through TFE3. In MiTF/TFE family, TFEB was the first and mostly studied one identified as a master regulator of lysosomal biogenesis.[52] In contrast, the impact of TFE3 on lysosome biogenesis has been discovered recently.[53,54] In this study, we confirmed its function in AML cells. However, the relationship of HA-induced cell-cycle arrest and lysosome accumulation is still ambiguous. In a previous study, genetic inactivation of CDK4/6, the kinases that drives G1-S transition, retains the nuclear localization and activation of TFEB and TFE3, which subsequently enhance lysosome biogenesis.[53] Whether the combination venetoclax and HA treatment induce lysosome biogenesis through a cell cycle regulators-TFEB/TFE3 axis requires future investigation.

Under the effect of venetoclax and HA, several lysosome-containing cathepsins were also overexpressed e.g., CTSD, CTSW, and CTSA. The release of proteases following lysosomal membrane leakage has been associated with several types of cell death, including necrosis, apoptosis, and pyroptosis depending on the extent of the leakage and the cellular context. In this study, we observed a prominent increase in cleaved caspase-3, which indicates apoptosis. Nevertheless, the combination HA and venetoclax may induce other forms of cell death. We found that combined treatment induces a significant increase in Annexin V^+/PI^+ cells, indicating necrosis. However, as indicated by rescue assay with Z-VAD-fmk and Necrostatin-1, apoptosis is the major form of cell death induced by the combinatory regime than necroptosis. Of note, inhibition of CTSD only slightly rescued the apoptosis induced by HA and venetoclax. This result might be due to the burst release of hydrolases in a short period of time due to lysosomal rupture. Thus, inhibition of one of these enzymes is insufficient to reverse cell death progression.

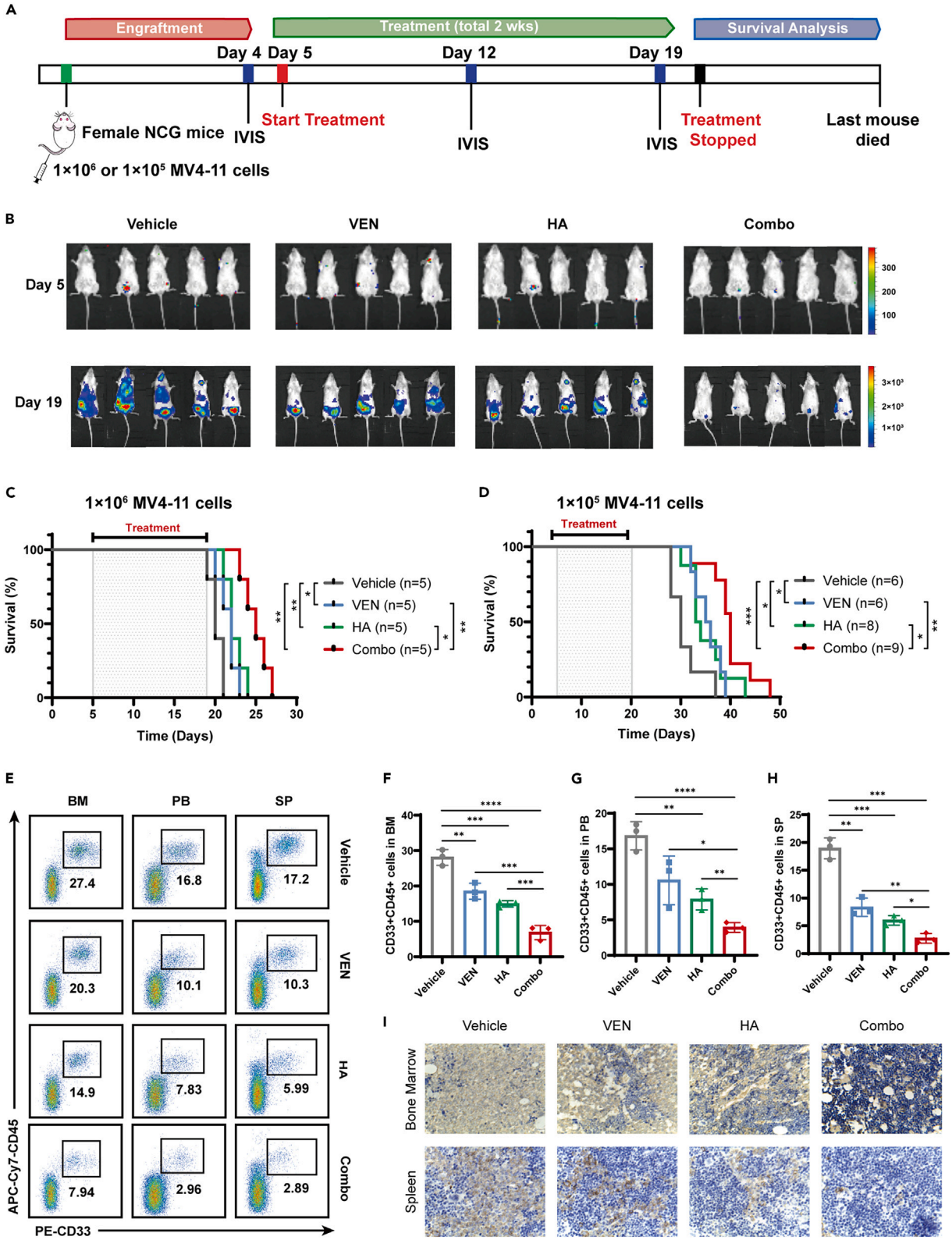
A
Engraftment
Treatment (total 2 wks)
Survival Analysis
Day 4
Day 5
Day 12
Day 19
Female NCG mice
1×10⁶ or 1×10⁵ MV4-11 cells
IVIS
Start Treatment
IVIS
IVIS
Treatment Stopped
Last mouse died
B
Vehicle
VEN
HA
Combo
Day 5
Day 19
300
200
100
3×10³
2×10³
1×10³
C
1×10⁶ MV4-11 cells
Treatment
Survival (%)
Time (Days)
Vehicle (n=5)
VEN (n=5)
HA (n=5)
Combo (n=5)
D
1×10⁵ MV4-11 cells
Treatment
Survival (%)
Time (Days)
Vehicle (n=6)
VEN (n=6)
HA (n=8)
Combo (n=9)
E
BM
PB
SP
Vehicle
VEN
HA
Combo
27.4
16.8
17.2
20.3
10.1
10.3
14.9
7.83
5.99
7.94
2.96
2.89
APC-Cy7-CD45
PE-CD33
F
CD33+CD45+ cells in BM
G
CD33+CD45+ cells in PB
H
CD33+CD45+ cells in SP
Vehicle
VEN
HA
Combo
I
Vehicle
VEN
HA
Combo
Bone Marrow
Spleen

Figure 5. HA combined with venetoclax eradicates AML in a xenograft model

(A) Schematic diagram of the experimental design.

(B) *In vivo* bioluminescence imaging of NCG mice before treatment (on Day 5) and after 2 weeks of treatment with vehicle, VEN (50 mg/kg), HA (20 mg/kg), or Combo (on Day 19).

(C and D) Overall survival of mice injected with 1×10^6 MV4-11 cells (C, n = 5 per group) or 1×10^5 MV4-11 cells (D, n = 6 per group) from each treatment group. VEN (50 mg/kg, orally) treatment and HA treatment (20 mg/kg, orally or intraperitoneally) for 2 weeks significantly prolongs survival of leukemic mice. The p values were calculated using a log rank (Mantel-Cox) test.

(E–H) Representative flow cytometry images (E) and statistical analysis of the percentage of human CD33/hCD45$^+$ (hCD33$^+$/hCD45$^+$) cells in the BM (F), PB (G), and SP (H).

(I) Representative images of infiltration in the BM and SP as analyzed by immunohistochemistry (IHC) staining of human CD45 (hCD45). Scale bar, 50 μm. Data are presented as the mean ± SD, and differences were compared one-way ANOVA. *, $p < 0.05$, **, $p < 0.01$, ***, $p < 0.001$, ****, $p < 0.0001$.

Combination regimens including HA and other drugs have already been explored. Shin Young Hyun et al. revealed that HA modulates sensitivity to Ara-C.[55] Moreover, in FLT3-ITD$^+$ AML, induction of sorafenib resistance significantly increases HA sensitivity. HA treatment of primary FLT3-ITD$^+$ AML cells significantly reduces leukemia initiation in anti-CD122-primed NOD/SCID mouse xenotransplants.[19] To explore whether the synergy between HA and venetoclax is restricted to cells harboring FLT3-ITD mutation, we added three FLT3-WT cell lines and found synergy of HA with venetoclax is not dependent on FLT3 mutation. Besides, most primary AML patients (12/14) sample we tested don't carry FLT3 mutation. Therefore, FLT3 mutation status doesn't seem to affect the synergistic effect of venetoclax and HA. Another fact that should be mentioned is the cell lines used in this study are mostly monocytic AML cell lines, so the synergistic effect of HA with venetoclax may be related to the cell type. However, only 6/15 AML patients whose bone marrow samples were collected and tested for synergistic effect were diagnosed as M4/M5 subtypes (French-American-British [FAB] classes), so the synergistic effect of HA and venetoclax may be expected for all AML subtypes. In a recent published study by Cheuk Him Man et al., amiloride used as a NHE1 inhibitor was potential to reduce leukemic burden *in vivo*, implying targeting NHE1 is a feasible strategy.[20] However, direct evaluation of the safety and effectiveness of HA *in vivo* is lacking. Here, we demonstrate the therapeutic potential of HA combined with venetoclax in an AML cell-derived xenograft model. HA and venetoclax treatment alleviates leukemia burden and prolongs survival, providing concrete evidence that HA could be an alternative for a combinatory regimen with venetoclax. Overall, our work defines the synergistic effects of HA and venetoclax *in vivo*, which is a promising strategy that deserves further investigation.

In summary, our findings identify NHE1 as a promising therapeutic target in AML and demonstrate that its inhibitor HA exerts potent anti-leukemia effects by modifying the cell cycle. In addition, we provide evidence for a novel therapeutic strategy by combination of HA with venetoclax, which increases lysosomal biogenesis by TFE3 and facilitates LMP. Taken together, our results provide evidence that warrants the exploration of HA in combinatory regimens for AML therapy.

Limitations of the study

This study still has several limitations. First, the mechanism of intracellular acidification and cell-cycle arrest induced by HA treatment is unclear. Second, this study focuses mainly on lysosome alterations in AML cells upon HA combined with Venetoclax treatment, while other two top pathways shown in KEGG enrichment, cell cycle and MAPK signaling pathway require further study for their contributions to synergism and links to lysosome alterations. Additionally, the clinical relevance of this study needs to be strengthened. More AML patient samples with diverse mutations or FAB subtypes and patient-derived xenograft murine model are needed to better illustrate the efficacy of the combination of HA and Venetoclax.

STAR★METHODS

Detailed methods are provided in the online version of this paper and include the following:

- KEY RESOURCES TABLE
- RESOURCE AVAILABILITY
  - Lead contact
  - Materials availability
  - Data and code availability
- EXPERIMENTAL MODEL AND STUDY PARTICIPANT DETAILS
  - Human samples
  - Cell lines
  - Animal models
- METHOD DETAILS
  - Quantitative real-time PCR
  - Viability assay
  - Apoptosis analysis
  - Western blotting
  - Cell cycle analysis

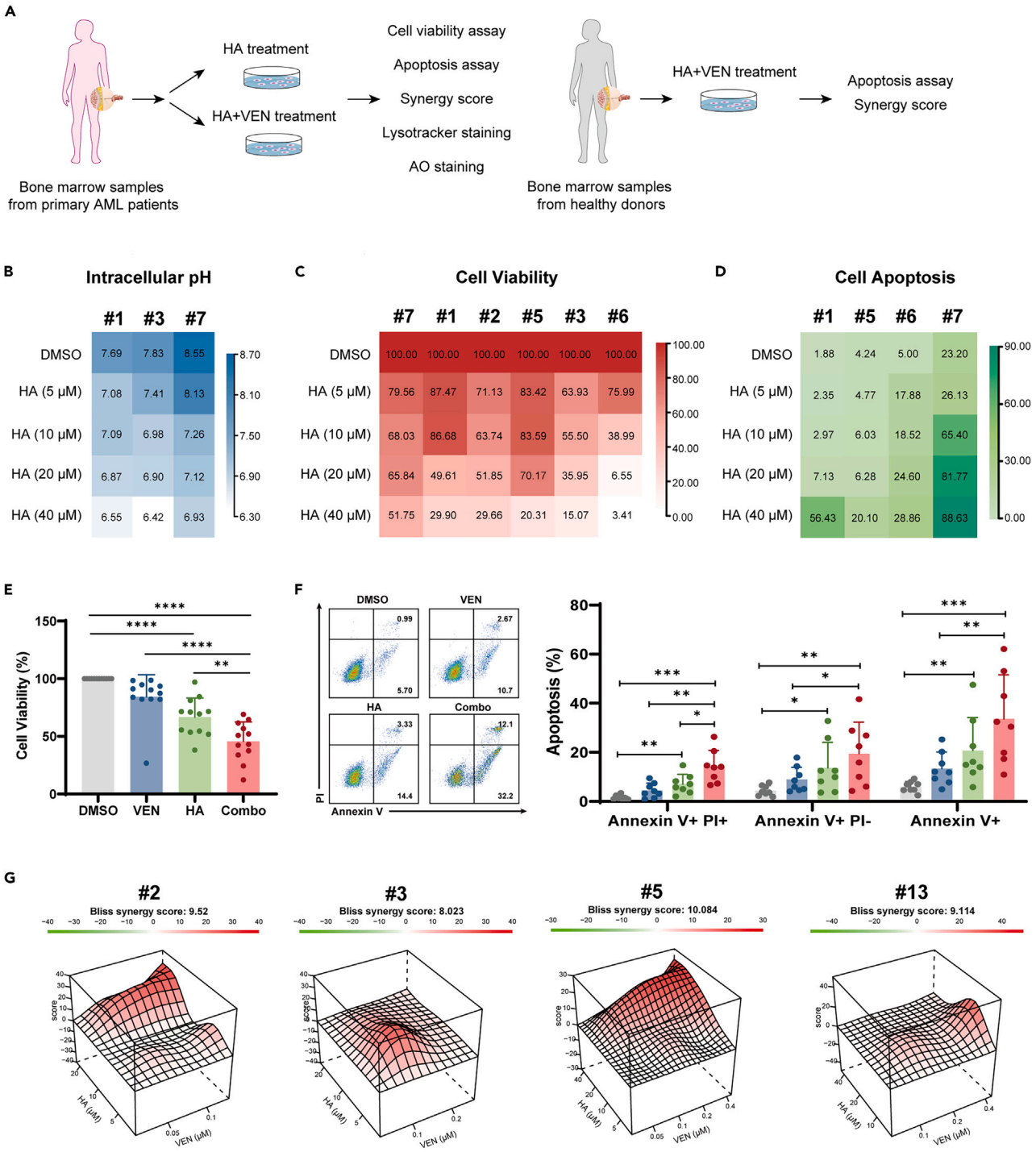

Figure 6. HA enhances the antileukemic effects of venetoclax in AML patient samples

(A) Schematic diagram of the experimental design.

(B–D) Primary AML blasts were treated with increasing concentrations of HA (0, 5 μM, 10 μM, 20 μM, and 40 μM) for 48 h and collected to measure pHi (B), cell viability (C), and apoptosis (D).

(E and F) Primary AML blasts were cultured in the presence of VEN or HA alone or combination for 48 h. Cell viability was measured by CCK8 assay (E), and apoptosis was detected by Annexin V/PI staining (F).

Figure 6. *Continued*

(G) Bliss synergy model of primary cells treated with different concentrations of VEN and HA. Primary cells from four newly diagnosed AML patients were treated with increasing doses of VEN and HA for 48 h to determine effects on cell viability. The presence of synergy was determined using SynergyFinder, and the Bliss synergy index is denoted as the red regions in the graphs. Data are presented as the mean ± SD, and differences were compared one-way ANOVA. *, $p < 0.05$, **, $p < 0.01$, ***, $p < 0.001$, ****, $p < 0.0001$.

- Measurement of intracellular pH
- Caspase3/7 activity assay
- EdU incorporation assay
- TUNEL staining
- Immunofluorescence
- Acridine orange staining
- Transmission electron microscopy
- Construction of MV4-11-luc$^+$ cells
- Cell transfection and lentiviral transduction
- RNA-seq analysis

● QUANTIFICATION AND STATISTICAL ANALYSIS

SUPPLEMENTAL INFORMATION

Supplemental information can be found online at https://doi.org/10.1016/j.isci.2023.108691.

ACKNOWLEDGMENTS

We were very grateful to Dr. Yangqiu Li, Dr. Yu Lan and Dr. Min Lu for critically reading the manuscript. We also thank Mr. Huien Zhan for sample collection.

Funding information.

This study was supported by the National Natural Science Foundation of China (Grant No. 81970143, No. 82270167), the Talent Young Program of Guangdong Province (2021B1515020017), and the Leading Talents Program from The First Affiliated Hospital of Jinan University to H.Z.

AUTHOR CONTRIBUTIONS

H.Z. designed the project, X.J. performed most experiments, K.H., X.S., Y.L., and L.H. F.L. performed other essential experiments, X.J., R.H., J.D., and H.Z. analyzed the data, X.J., J.D., and Z.H. wrote and revised the manuscript. All authors have read and H.Z. approved the final submitted manuscript.

DECLARATION OF INTERESTS

The authors declare no conflict of interest.

Received: July 11, 2023
Revised: October 15, 2023
Accepted: December 5, 2023
Published: December 8, 2023

REFERENCES

1. Estey, E. (2016). Acute Myeloid Leukemia - Many Diseases, Many Treatments. N. Engl. J. Med. *375*, 2094–2095.
2. DiNardo, C.D., Pratz, K.W., Letai, A., Jonas, B.A., Wei, A.H., Thirman, M., Arellano, M., Frattini, M.G., Kantarjian, H., Popovic, R., et al. (2018). Safety and preliminary efficacy of venetoclax with decitabine or azacitidine in elderly patients with previously untreated acute myeloid leukaemia: a non-randomised, open-label, phase 1b study. Lancet Oncol. *19*, 216–228.
3. DiNardo, C.D., Pratz, K., Pullarkat, V., Jonas, B.A., Arellano, M., Becker, P.S., Frankfurt, O., Konopleva, M., Wei, A.H., Kantarjian, H.M., et al. (2019). Venetoclax combined with decitabine or azacitidine in treatment-naive, elderly patients with acute myeloid leukemia. Blood *133*, 7–17.
4. Taylor, S., Spugnini, E.P., Assaraf, Y.G., Azzarito, T., Rauch, C., and Fais, S. (2015). Microenvironment acidity as a major determinant of tumor chemoresistance: Proton pump inhibitors (PPIs) as a novel therapeutic approach. Drug Resist. Updat. *23*, 69–78.
5. Corbet, C., and Feron, O. (2017). Tumour acidosis: from the passenger to the driver's seat. Nat. Rev. Cancer *17*, 577–593.
6. Neri, D., and Supuran, C.T. (2011). Interfering with pH regulation in tumours as a therapeutic strategy. Nat. Rev. Drug Discov. *10*, 767–777.
7. Reshkin, S.J., Bellizzi, A., Caldeira, S., Albarani, V., Malanchi, I., Poignee, M., Alunni-Fabbroni, M., Casavola, V., and Tommasino, M. (2000). Na+/H+ exchanger-dependent intracellular alkalinization is an early event in malignant transformation and plays an essential role in the development of subsequent transformation-associated phenotypes. Faseb. J. *14*, 2185–2197.
8. Guan, X., Luo, L., Begum, G., Kohanbash, G., Song, Q., Rao, A., Amankulor, N., Sun, B., Sun, D., and Jia, W. (2018). Elevated Na/H exchanger 1 (SLC9A1) emerges as a marker for tumorigenesis and prognosis in gliomas. J. Exp. Clin. Cancer Res. *37*, 255.
9. Hasan, M.N., Luo, L., Ding, D., Song, S., Bhuiyan, M.I.H., Liu, R., Foley, L.M., Guan, X., Kohanbash, G., Hitchens, T.K., et al. (2021). Blocking NHE1 stimulates glioma tumor immunity by restoring OXPHOS

function of myeloid cells. Theranostics *11*, 1295–1309.
10. Amith, S.R., and Fliegel, L. (2017). Na(+)/H(+) exchanger-mediated hydrogen ion extrusion as a carcinogenic signal in triple-negative breast cancer etiopathogenesis and prospects for its inhibition in therapeutics. Semin. Cancer Biol. *43*, 35–41.
11. Jia, Y., Liu, W., Zhan, H.E., Yi, X.P., Liang, H., Zheng, Q.L., Jiang, X.Y., Zhou, H.Y., Zhao, L., Zhao, X.L., and Zeng, H. (2020). Roles of hsa-miR-12462 and SLC9A1 in acute myeloid leukemia. J. Hematol. Oncol. *13*, 101.
12. Chen, Q., Liu, Y., Zhu, X.L., Feng, F., Yang, H., and Xu, W. (2019). Increased NHE1 expression is targeted by specific inhibitor cariporide to sensitize resistant breast cancer cells to doxorubicin *in vitro* and *in vivo*. BMC Cancer *19*, 211.
13. Park, K.S., Poburko, D., Wollheim, C.B., and Demaurex, N. (2009). Amiloride derivatives induce apoptosis by depleting ER Ca(2+) stores in vascular endothelial cells. Br. J. Pharmacol. *156*, 1296–1304.
14. Jiang, K., Xu, Y., Wang, D., Chen, F., Tu, Z., Qian, J., Xu, S., Xu, Y., Hwa, J., Li, J., et al. (2022). Cardioprotective mechanism of SGLT2 inhibitor against myocardial infarction is through reduction of autosis. Protein Cell *13*, 336–359.
15. Galluzzi, L., Bravo-San Pedro, J.M., and Kroemer, G. (2014). Organelle-specific initiation of cell death. Nat. Cell Biol. *16*, 728–736.
16. Ohkuma, S., Moriyama, Y., and Takano, T. (1982). Identification and characterization of a proton pump on lysosomes by fluorescein-isothiocyanate-dextran fluorescence. Proc. Natl. Acad. Sci. USA *79*, 2758–2762.
17. Sukhai, M.A., Prabha, S., Hurren, R., Rutledge, A.C., Lee, A.Y., Sriskanthadevan, S., Sun, H., Wang, X., Skrtic, M., Seneviratne, A., et al. (2013). Lysosomal disruption preferentially targets acute myeloid leukemia cells and progenitors. J. Clin. Invest. *123*, 315–328.
18. Tang, Z., Li, C., Kang, B., Gao, G., Li, C., and Zhang, Z. (2017). GEPIA: a web server for cancer and normal gene expression profiling and interactive analyses. Nucleic Acids Res. *45*. W98-w102.
19. Man, C.H., Lam, S.S.Y., Sun, M.K.H., Chow, H.C.H., Gill, H., Kwong, Y.L., and Leung, A.Y.H. (2014). A novel tescalcin-sodium/hydrogen exchange axis underlying sorafenib resistance in FLT3-ITD+ AML. Blood *123*, 2530–2539.
20. Man, C.H., Zeng, X., Lam, W., Ng, T.C.C., Kwok, T.H., Dang, K.C.C., Leung, T.W.Y., Ng, N.K.L., Lam, S.S.Y., Cher, C.Y., and Leung, A.Y.H. (2022). Regulation of proton partitioning in kinase-activating acute myeloid leukemia and its therapeutic implication. Leukemia *36*, 1990–2001.
21. Geeleher, P., Cox, N., and Huang, R.S. (2014). pRRophetic: an R package for prediction of clinical chemotherapeutic response from tumor gene expression levels. PLoS One *9*, e107468.
22. Ballabio, A., and Bonifacino, J.S. (2020). Lysosomes as dynamic regulators of cell and organismal homeostasis. Nat. Rev. Mol. Cell Biol. *21*, 101–118.
23. Postovit, L., Widmann, C., Huang, P., and Gibson, S.B. (2018). Harnessing Oxidative Stress as an Innovative Target for Cancer Therapy. Oxid. Med. Cell. Longev. *2018*, 6135739.
24. Piao, S., and Amaravadi, R.K. (2016). Targeting the lysosome in cancer. Ann. N. Y. Acad. Sci. *1371*, 45–54.
25. Aits, S., Kricker, J., Liu, B., Ellegaard, A.M., Hämälistö, S., Tvingsholm, S., Corcelle-Termeau, E., Høgh, S., Farkas, T., Holm Jonassen, A., et al. (2015). Sensitive detection of lysosomal membrane permeabilization by lysosomal galectin puncta assay. Autophagy *11*, 1408–1424.
26. Kimura, T., Takabatake, Y., Takahashi, A., and Isaka, Y. (2013). Chloroquine in cancer therapy: a double-edged sword of autophagy. Cancer Res. *73*, 3–7.
27. Wang, F., Gómez-Sintes, R., and Boya, P. (2018). Lysosomal membrane permeabilization and cell death. Traffic (Copenhagen, Denmark) *19*, 918–931.
28. DiGiammarino, E.L., Lee, A.S., Cadwell, C., Zhang, W., Bothner, B., Ribeiro, R.C., Zambetti, G., and Kriwacki, R.W. (2002). A novel mechanism of tumorigenesis involving pH-dependent destabilization of a mutant p53 tetramer. Nat. Struct. Biol. *9*, 12–16.
29. Man, C.H., Mercier, F.E., Liu, N., Dong, W., Stephanopoulos, G., Jiang, L., Jung, Y., Lin, C.P., Leung, A.Y.H., and Scadden, D.T. (2022). Proton export alkalinizes intracellular pH and reprograms carbon metabolism to drive hematopoietic progenitor growth. Blood *139*, 502–522.
30. Aredia, F., Giansanti, V., Mazzini, G., Savio, M., Ortiz, L.M.G., Jaadane, I., Zaffaroni, N., Forlino, A., Torriglia, A., and Scovassi, A.I. (2013). Multiple effects of the Na(+)/H (+) antiporter inhibitor HMA on cancer cells. Apoptosis *18*, 1586–1598.
31. Rolver, M.G., Elingaard-Larsen, L.O., Andersen, A.P., Counillon, L., and Pedersen, S.F. (2020). Pyrazine ring-based Na(+)/H(+) exchanger (NHE) inhibitors potently inhibit cancer cell growth in 3D culture, independent of NHE1. Sci. Rep. *10*, 5800.
32. Buckley, B.J., Aboelela, A., Majed, H., Bujaroski, R.S., White, K.L., Powell, A.K., Wang, W., Katneni, K., Saunders, J., Shackleford, D.M., et al. (2021). Systematic evaluation of structure-property relationships and pharmacokinetics in 6-(hetero)aryl-substituted matched pair analogs of amiloride and 5-(N,N-hexamethylene)amiloride. Bioorg. Med. Chem. *37*, 116116.
33. Aredia, F., Czaplinski, S., Fulda, S., and Scovassi, A.I. (2016). Molecular features of the cytotoxicity of an NHE inhibitor: Evidence of mitochondrial alterations, ROS overproduction and DNA damage. BMC Cancer *16*, 851.
34. Tschöp, K., Müller, G.A., Grosche, J., and Engeland, K. (2006). Human cyclin B3. mRNA expression during the cell cycle and identification of three novel nonclassical nuclear localization signals. FEBS J. *273*, 1681–1695.
35. Wang, J., Song, C., Cao, X., Li, H., Cai, H., Ma, Y., Huang, Y., Lan, X., Lei, C., Ma, Y., et al. (2019). MiR-208b regulates cell cycle and promotes skeletal muscle cell proliferation by targeting CDKN1A. J. Cell. Physiol. *234*, 3720–3729.
36. Laresgoiti, U., Apraiz, A., Olea, M., Mitxelena, J., Osinalde, N., Rodriguez, J.A., Fullaondo, A., and Zubiaga, A.M. (2013). E2F2 and CREB cooperatively regulate transcriptional activity of cell cycle genes. Nucleic Acids Res. *41*, 10185–10198.
37. Xie, R., Wang, H., Jin, H., Wen, G., Tuo, B., and Xu, J. (2017). NHE1 is upregulated in gastric cancer and regulates gastric cancer cell proliferation, migration and invasion. Oncol. Rep. *37*, 1451–1460.
38. Sun, Z., Luan, S., Yao, Y., Qin, T., Xu, X., Shen, Z., Yao, R., and Yue, L. (2020). NHE1 Mediates 5-Fu Resistance in Gastric Cancer via STAT3 Signaling Pathway. OncoTargets Ther. *13*, 8521–8532.
39. Rich, I.N., Worthington-White, D., Garden, O.A., and Musk, P. (2000). Apoptosis of leukemic cells accompanies reduction in intracellular pH after targeted inhibition of the Na(+)/H(+) exchanger. Blood *95*, 1427–1434.
40. Flinck, M., Kramer, S.H., and Pedersen, S.F. (2018). Roles of pH in control of cell proliferation. Acta Physiol. *223*, e13068.
41. Gerson, D.F., Kiefer, H., and Eufe, W. (1982). Intracellular pH of mitogen-stimulated lymphocytes. Science (New York, N.Y.) *216*, 1009–1010.
42. Pouysségur, J., Chambard, J.C., Franchi, A., Paris, S., and Van Obberghen-Schilling, E. (1982). Growth factor activation of an amiloride-sensitive Na+/H+ exchange system in quiescent fibroblasts: coupling to ribosomal protein S6 phosphorylation. Proc. Natl. Acad. Sci. USA *79*, 3935–3939.
43. Moolenaar, W.H., Tsien, R.Y., van der Saag, P.T., and de Laat, S.W. (1983). Na+/H+ exchange and cytoplasmic pH in the action of growth factors in human fibroblasts. Nature *304*, 645–648.
44. Chambard, J.C., and Pouyssegur, J. (1986). Intracellular pH controls growth factor-induced ribosomal protein S6 phosphorylation and protein synthesis in the G0——G1 transition of fibroblasts. Exp. Cell Res. *164*, 282–294.
45. Pouysségur, J., Franchi, A., L'Allemain, G., and Paris, S. (1985). Cytoplasmic pH, a key determinant of growth factor-induced DNA synthesis in quiescent fibroblasts. FEBS Lett. *190*, 115–119.
46. Man, C.H., Mercier, F.E., Liu, N., Dong, W., Stephanopoulos, G., Jiang, L., Jung, Y., Lin, C.P., Leung, A.Y.H., and Scadden, D.T. (2022). Proton export alkalinizes intracellular pH and reprograms carbon metabolism to drive normal and malignant cell growth. Blood *139*, 502–522.
47. Jones, C.L., Stevens, B.M., D'Alessandro, A., Reisz, J.A., Culp-Hill, R., Nemkov, T., Pei, S., Khan, N., Adane, B., Ye, H., et al. (2019). Inhibition of Amino Acid Metabolism Selectively Targets Human Leukemia Stem Cells. Cancer Cell *35*, 333–335.
48. Lin, K.H., Xie, A., Rutter, J.C., Ahn, Y.R., Lloyd-Cowden, J.M., Nichols, A.G., Soderquist, R.S., Koves, T.R., Muoio, D.M., MacIver, N.J., et al. (2019). Systematic Dissection of the Metabolic-Apoptotic Interface in AML Reveals Heme Biosynthesis to Be a Regulator of Drug Sensitivity. Cell Metab. *29*, 1217–1231.e7.
49. Lagadinou, E.D., Sach, A., Callahan, K., Rossi, R.M., Neering, S.J., Minhajuddin, M., Ashton, J.M., Pei, S., Grose, V., O'Dwyer, K.M., et al. (2013). BCL-2 inhibition targets oxidative phosphorylation and selectively eradicates quiescent human leukemia stem cells. Cell Stem Cell *12*, 329–341.
50. Zhitomirsky, B., and Assaraf, Y.G. (2016). Lysosomes as mediators of drug resistance in cancer. Drug Resist. Updat. *24*, 23–33.
51. Rafiq, S., McKenna, S.L., Muller, S., Tschan, M.P., and Humbert, M. (2021). Lysosomes in

acute myeloid leukemia: potential therapeutic targets? Leukemia *35*, 2759–2770.

52. Raben, N., and Puertollano, R. (2016). TFEB and TFE3: Linking Lysosomes to Cellular Adaptation to Stress. Annu. Rev. Cell Dev. Biol. *32*, 255–278.
53. Yin, Q., Jian, Y., Xu, M., Huang, X., Wang, N., Liu, Z., Li, Q., Li, J., Zhou, H., Xu, L., et al. (2020). CDK4/6 regulate lysosome biogenesis through TFEB/TFE3. J. Cell Biol. *219*, e201911036.
54. Martina, J.A., Diab, H.I., Lishu, L., Jeong-A, L., Patange, S., Raben, N., and Puertollano, R. (2014). The nutrient-responsive transcription factor TFE3 promotes autophagy, lysosomal biogenesis, and clearance of cellular debris. Sci. Signal. *7*, ra9.
55. Hyun, S.Y., Na, E.J., Jang, J.E., Chung, H., Kim, S.J., Kim, J.S., Kong, J.H., Shim, K.Y., Lee, J.I., Min, Y.H., and Cheong, J.W. (2019). Induction of apoptosis and differentiation by Na/H exchanger 1 modulation in acute myeloid leukemia cells. Biochem. Biophys. Res. Commun. *519*, 887–893.

STAR★METHODS

KEY RESOURCES TABLE

REAGENT or RESOURCE	SOURCE	IDENTIFIER
Antibodies		
Caspase 3	Cell Signaling Technology	Cat# 9662; RRID:AB_331439
Cleaved-caspase 3	Cell Signaling Technology	Cat# 9661; RRID:AB_2341188
Phospho-p38	Cell Signaling Technology	Cat# 4511; RRID:AB_2139682
LAMP1	Proteintech	Cat# 21997-1-AP; RRID:AB_2878966
CTSD	Wanleibio	Cat# WL01234; RRID:AB_2313773
TFE3	Affinity	Cat# AF0363; RRID:AB_2833528
ACTIN	Proteintech	Cat# 66009-1-Ig; RRID:AB_2687938
Tubulin	Proteintech	Cat# 11224-1-AP; RRID:AB_2210206
Anti-rabbit IgG (H+L), F(ab')2 Fragment (Alexa Fluor 488 Conjugate)	Cell Signaling Technology	Cat# 4412; RRID:AB_1904025
Anti-rabbit IgG (H+L), F(ab')2 Fragment (Alexa Fluor 647 Conjugate)	Cell Signaling Technology	Cat# 4414; RRID:AB_10693544
Anti-human CD33 (HIM3-4) PE	eBioscience	Cat# 12-0339-42; RRID:AB_10855031
Anti-human CD45 (2D1) APC-Cy7	Biolegend	Cat# 368516; RRID:AB_2566376
Anti-human CD45 (D9M8I) Rabbit mAb	Cell Signaling Technology	Cat# 13917; RRID:AB_2750898
Biological samples		
Human bone marrow samples	This paper	N/A
Chemicals, peptides, and recombinant proteins		
Recombinant human SCF	Peprotech	Cat# 300-07
Recombinant human FLT3L	Peprotech	Cat# 300-19
Recombinant human IL-3	Peprotech	Cat# 200-03
Recombinant human IL-6	Peprotech	Cat# 200-06
Recombinant human TPO	Peprotech	Cat# 300-18
Venetoclax (VEN)	MedChemExpress	Cat# HY-15531
Hexamethylene amiloride (HA)	MedChemExpress	Cat# HY-128067
Pepstatin A	MedChemExpress	Cat# HY-P0018
Z-VAD-fmk	MedChemExpress	Cat# HY-16658B
Necrostatin-1	MedChemExpress	Cat# HY-15760
Acridine Orange	MedChemExpress	Cat# HY-101879
Lipofectamine 3000	ThermoFisher	Cat# L3000075
Polybrene	Biosharp	Cat# BL628A
VivoGlo™ Luciferin	Promega	Cat# P1041
Critical commercial assays		
CCK-8	Yeasen	Cat# 40203ES80
Apoptosis Assay kit	Biosharp	Cat# BL110A
Cell cycle Analysis kit	Beyotime	Cat# C1052
EdU Cell Proliferation Kit	Beyotime	Cat# C0071L
TUNEL BrightGreen Apoptosis Detection Kit	Vazyme	Cat# A112-03
Caspase 3/7 Activity Apoptosis Assay Kit	AAT Bioquest	Cat# 22796
Intracellular pH Calibration Buffer Kit	ThermoFisher	Cat# P35379

(*Continued on next page*)

Continued

REAGENT or RESOURCE	SOURCE	IDENTIFIER
Deposited data		
RNA-seq data for MV4-11 cells upon different treatments	This study	Accession number: GSE247175 https://www.ncbi.nlm.nih.gov/geo/
GEO RNA-seq data	GEO	https://www.ncbi.nlm.nih.gov/geo/
TCGA AML RNA-seq data	TCGA	https://gdc.cancer.gov/access-data
MILE dataset	MILE dataset	N/A
Experimental models: Cell lines		
MV4-11	ATCC	Cat# CRL-9591
MOLM13	CTCC	Cat# CTCC-007-0236
THP-1	ATCC	Cat# TIB-202
Kasumi-1	ATCC	Cat# CRL-2724
KG-1α	ATCC	Cat# CCL-246.1
293T	ATCC	Cat# CRL-3216
Experimental models: Organisms/strains		
NCG mice: NOD/ShiLtJGpt-Prkdcem26Cd52Il2rgem26Cd22/Gpt	GemPharmatech	NO. T001475
Oligonucleotides		
sgNHE1#1,GTTTGCCAACTACGAACACG	VectorBuilder	N/A
sgNHE1#2, CGGCTCGATGACCCGGATGT	VectorBuilder	N/A
sgNHE1#3, TGCCTCATCGCCCGCGTGCT	VectorBuilder	N/A
shTFE3#1, CCGGCAGCTCCGAATTCAGGAACTACTC GAGTAGTTCCTGAATTCGGAGCTGTTTTTGAATT	IGEBio	N/A
shTFE3#2, CCGGATTGTTGCTGACATAGAATTACTCG AGTAATTCTATGTCAGCAACAATTTTTTGAATT	IGEBio	N/A
shTFE3#3, CCGGGCCTGGAGTCCAGTTACAATGCTC GAGCATTGTAACTGGACTCCAGGCTTTTTGAATT	IGEBio	N/A
qPCR primers: CCNB3 Forward: ATGAAGGCAGTATGCAAGAAGG Reverse: CATCCACACGAGGTGAGTTGT	This study	N/A
qPCR primers: TTK Forward: GTGGAGCAGTACCACTAGAAATG Reverse: CCCAAGTGAACCGGAAAATGA	This study	N/A
qPCR primers: STAG2 Forward: TCCTTCTGGTCCAAACCGAAT Reverse: ACCGACTGCATAGCACTCTTG	This study	N/A
qPCR primers:CHEK1 Forward: ATATGAAGCGTGCCGTAGACT Reverse: TGCCTATGTCTGGCTCTATTCTG	This study	N/A
qPCR primers: CDKN1A Forward: TGTCCGTCAGAACCCATGC Reverse: AAAGTCGAAGTTCCATCGCTC	This study	N/A
qPCR primers: SMC3 Forward: AACATAATGTGATTGTGGGCAGA Reverse: TCCTTTTTGGCACCAATAACTCT	This study	N/A
qPCR primers: GADD45A Forward: GAGAGCAGAAGACCGAAAGGA Reverse: CACAACACCACGTTATCGGG	This study	N/A

(*Continued on next page*)

Continued

REAGENT or RESOURCE	SOURCE	IDENTIFIER
qPCR primers: STAG1 Forward: TGGCAGCGAGCTTGAAGAAA Reverse: CCACCTCAAATAATGTGACAGGC	This study	N/A
qPCR primers: PKMYT1 Forward: CATGGCTCCTACGGAGAGGT Reverse: ACATGGAACGCTTTACCGCAT	This study	N/A
qPCR primers: CDC25C Forward: TCTACGGAACTCTTCTCATCCAC Reverse: TCCAGGAGCAGGTTTAACATTTT	This study	N/A
qPCR primers: TFE3 Forward: CCGTGTTCGTGCTGTTGGA Reverse: GCTCGTAGAAGCTGTCAGGAT	This study	N/A
qPCR primers: ACTIN Forward: CATGTACGTTGCTATCCAGGC Reverse: CTCCTTAATGTCACGCACGAT	This study	N/A
Software and algorithms		
FlowJo Software	FlowJo	https://www.flowjo.com/solutions/flowjo/downloads
ImageJ	ImageJ	https://imagej.net/Downloads
Graphpad Prism 8.0	Graphpad Prism	https://www.graphpad.com/scientific-software/prism
R version 4.2.1	R Core Team	https://www.r-project.org
Compusyn 1.0.1	N/A	N/A

RESOURCE AVAILABILITY

Lead contact

Further information and requests for resources and reagents should be directed to and will be fulfilled by the lead contact, Hui Zeng (androps2011@hotmail.com).

Materials availability

This study did not generate new unique reagents. All materials in this study are commercially available.

Data and code availability

- The raw and processed sequence data reported in this paper have been deposited in the Gene Expression Omnibus under accession number GSE247175. The accession numbers for the public datasets used in this paper are listed in the key resources table.
- This paper does not report original code.
- Any additional information required to reanalyze the data reported in this paper is available from the lead contact upon request.

EXPERIMENTAL MODEL AND STUDY PARTICIPANT DETAILS

Human samples

Human bone marrow (BM) samples from Chinese AML patients and healthy donors were collected according to a protocol approved by the Institutional Review Board of The First Affiliated Hospital of Jinan University (IRB, approval number: KYk-2021-030), with patients informed consent acquired in accordance with the Declaration of Helsinki. The main clinical characteristics are shown in Table S1. Mononuclear cells were isolated by density-gradient centrifugation (Ficoll-Paque, Solarbio, China) and cultured in a base media of MEM (Gibco) supplemented with 10nM human cytokines SCF, IL3, FLT, IL6 and TPO (PEPROTech). The media was supplemented with 20% fetal bovine serum (BI) and 1% penicillin/streptomycin (Gibco). Cells were then subjected to apoptosis analysis, proliferation analysis, and flow cytometry analysis.

Cell lines

MV4-11, MOLM13, THP-1, Kasumi-1 and KG-1α were cultured in RPMI 1640 medium (Gibco). All media contained 10% fetal bovine serum (BI) plus 1% penicillin/streptomycin (Gibco). Cells were maintained in a 37°C humidified atmosphere containing 5% CO2. Cell lines were

authenticated using Short Tandem Repeat (STR) analysis as described in 2012 in ANSI Standard (ANSI/ATCC ASN-0002-2011 Authentication of Human Cell Lines: Standardization of STR Profiling) by the ATCC Standards Development Organization (SDO). Cells were routinely tested for mycoplasma contamination and were negative.

Animal models

Animal experiments were conducted in a specific pathogen-free facility at Laboratory Animal Center of Jinan University. Six- to eight-week-old NOD/SCID female mice were obtained from GemPharmatech (Guangdong, China). On day 0, each mouse was injected intravenously with 1×10^6 or 1×10^5 MV4-11 cells. On day 4, mice were randomly distributed into four groups: vehicle control, VEN (50 mg/kg), HA (20 mg/kg), or combination (HA 20 mg/kg plus VEN 50 mg/kg). VEN was administered orally and HA was administered orally or intraperitoneally. The treatment was started from day 5 for a "5 days on, 2 days off" scheme for 2 cycles. Mice were weighed every two days. Three-four mice in each group were humanely euthanized after 2 treatment cycles. Bone marrow, liver, and spleen were harvested for flow cytometric measurements and immunohistochemistry analysis. Other mice were kept until the survival end point. All animal experiments were approved by and performed according to the guidelines of the Institutional Animal Care and Use Committee of of Jinan University (IACUC-JNU, approval number: 20221028-03).

METHOD DETAILS

Quantitative real-time PCR

Total RNA was extracted using TRIzol (Life Technologies). cDNA was prepared using 2 μg of total RNA plus random hexamer primers with the Evo M-MLV RT Kit (Accurate Biology). Quantification of transcripts was performed via the SYBR® Green Premix Pro Taq HS qPCR Kit (Accurate Biology) according to the manufacturer's instructions. Real-time PCR results are presented as the mean of three independent experiments normalized to ACTIN transcripts. Fold changes were calculated using the ΔΔCt method.

Viability assay

Cells were seeded in 96-well plates at 40,000 cells per well in 100 μL. Inhibitors were added, and the cells were incubated at 37°C for 24, 48, and 72 h. Cell viability was measured using Cell Counting Kit-8 (CCK-8, MedChemExpress, Shanghai, China) according to the manufacturer's instructions. Each experiment was performed in triplicate. The extent and direction of the antileukemic interaction between the two agents were determined by calculating the combination index (CI) using CompuSyn software (Combosyn Inc., Paramus, NJ, USA), in which $CI < 1$, $CI = 1$, and $CI > 1$ are respectively indicative of synergistic, additive, and antagonistic effects.

Apoptosis analysis

Cells were seeded at a density of 2×10^5 cells/mL in the presence or absence of inhibitors for 48 h. Harvested cells were washed and resuspended in binding buffer containing Annexin V-FITC and propidium iodide (PI) (BD Biosciences, Bedford, MA). After incubation for 15 min, the samples were subjected to FACS analysis using a BD FACSCanto II flow cytometer (BD Biosciences, Bedford, MA). Apoptotic cells were analyzed with FlowJo software (Version 9.9.3, Tree Star), and the results are presented as the percentage of cells that were apoptotic (annexin V^+ PI^- or annexin V^+ PI^+).

Western blotting

Total protein was extracted from cells pellets using NP-40 Buffer (Beyotime, China) supplemented with protease and phosphatase inhibitors (New Cell and Molecular Biotech, Suzhou, China). Protein concentrations were measured using the BCA Protein Assay Kit (Beyotime, China). Western blotting analysis was performed as previously described. Targeted proteins were visualized by incubation with an enhanced chemiluminescence reagent on autoradiography film. Densitometry measurements were made using Image J, and normalization to ACTIN or Tubulin was performed.

Cell cycle analysis

A total of 5×10^5 cells were seeded into each well of a six-well plate, and the cells were treated for 48 h with indicated inhibitors. Cells were pelleted by centrifugation (1,000 × rpm, RT, 5 min) and resuspended in 0.2 mL PBS. Cells were fixed in ice-cold 70% (v/v) ethanol/PBS overnight at 4°C. Samples were then centrifuged (1,000 × rpm, 4°C, 5 min), washed with PBS, and resuspended in 0.25 mL PBS containing 50 μg/ml PI, 0.1 mg/ml RNaseA (Beyotime, China). Following 30 min incubation at 37°C in the dark, cell cycle profiles were acquired with a FACSCanto II (BD Biosciences). Data were analyzed using FlowJo (FlowJo, USA) software.

Measurement of intracellular pH

MV4-11 and MOLM13 cell lines were seeded in 24-well plates with and without inhibitors 48 h prior to experiments. They were then incubated with 5 μM BCECF-AM (Beyotime) for 30 min at 37°C. Cells were washed twice in PBS and placed in MultiScan FC (ThermoFisher). The cells were excited at the 440 and 495 nm wavelengths, and a 440/495 ratio was detected at 535 nm. A pH standard curve was created using the Intracellular pH Calibration Buffer Kit (ThermoFisher).

Caspase3/7 activity assay

Following treatments of cells, caspase 3/7 activity assays were performed using the Cell Meter™ Caspase 3/7 Activity Apoptosis Assay Kit (AAT Bioquest) according to the manufacturer's description. The activity was measured by FACS analysis using a 488 nm laser with 530/30 (GREEN) using FACSCanto II (BD Biosciences).

EdU incorporation assay

Cell proliferation was detected according to manufacturer's instructions. Briefly, cells were seeded in 24 well plates (1×10^5 cells/well) and incubated with 50 μM EdU for 2 h at 37°C. Then, the cells were immobilized and washed. After EdU staining, cells were stained with Hoechst 33342. The percentage of EdU+ cells was calculated from five random fields in three wells.

TUNEL staining

The TUNEL Universal Apoptosis Detection Kit (Vazyme) was used for the detection of fragmented DNA in the nucleus by green fluorescence probe labeling during apoptosis. After 48 h exposure to inhibitors, cells were analyzed for apoptotic cells according to the manufacturer's instructions. Briefly, cells were fixed with 4% (w/v) paraformaldehyde for 10 min and permeabilized with 0.3% Triton X-100 in PBS for 5 min at RT. Cells were washed and stained for TUNEL assay in PBS for 1 h, and nuclei were visualized with DAPI (Sigma). The number of TUNEL-positive cells in each section were counted in five random fields using ImageJ software.

Immunofluorescence

After the desired treatment, MV4-11 cells were washed with PBS, fixed in 4% (w/v) paraformaldehyde for 20 min, permeabilized in 0.2% (v/v) Triton X-100 for 30 minutes, and blocked for 1 hour in 3% BSA. Fixed and permeabilized cells were then incubated with appropriate primary antibodies in PBS + 1% BSA overnight at 4°C, washed and stained with fluorescence-conjugated secondary antibodies (1:1,000) for 1 hour at room temperature. The cells were washed three times, and a final concentration of 2 μg/mL DAPI (Sigma) was included in the final washing to stain nuclei. Images were captured using a Zeiss LSM880 Airyscan confocal microscope using a 100 X objective (N.A. 1.46).

Acridine orange staining

Cells were washed with PBS and resuspended in RPMI 1640 plus 10% FBS containing 5 ug/mL Acridine Orange (MCE) to a concentration of 2×10^5 cells per ml. Cells were then incubated at 37°C for 20 min and washed three times with PBS. Acridine Orange staining was measured by FACS analysis using a 488 nm laser with 530/30 (GREEN) and 695/40 (RED) filters using FACSCanto II (BD Biosciences).

Transmission electron microscopy

MV4-11, MOLM13 and THP-1 cells were collected and fixed with Electron Microscope Fixative at 4°C overnight. After incubation, the cells were washed three times with phosphate buffer followed by post-fixation in 1% osmium tetroxide at room temperature for 2 h. The samples were dehydrated and then stained with 2% aqueous uranyl acetate. The structures of the lysosome were observed under a HT7700 transmission electron microscope (Hitachi, Tokyo, Japan) operated at 80 kV.

Construction of MV4-11-luc$^+$ cells

pCDH-CMV-Luciferase-EF1-GFP-T2A-Puro lentiviral vectors were purchased from IGEbio (Guangzhou, China). For stable GFP and luciferase expression, $2x10^5$ MV4-11 cells were seeded in 24-well plates in 1 ml RPMI 1640 and infected with lentivirus and 5 μL polybrene for 12 h. Cells were then recovered in complete RPMI 1640 for 48 h and sorted for GFP+ cells.

Cell transfection and lentiviral transduction

To make LGALS3-GFP-expressing MV4-11 cells, LGALS3-GFP plasmid was purchased from IGEbio (Guangdong, China). To construct sgNHE1 and shTFE3 cell lines, three different sgRNA sequences special for NHE1 in lentiviral vector pLV[CRISPR]-hCas9:T2A:Puro-U6-sgRNA were purchased from VectorBuilder and three different shRNA sequences special for TFE3 and a scramble shRNA in lentiviral vector pLKO.1-U6-EF1a-copGFP-T2A-puro were purchased from IGEbio.

For viral packaging, plasmid was co-transfected together with psPAX2 and pMD2.G into the 293T cells using Lipo3000 (Invitrogen) and co-precipitation at 8:6:4 μg (for a 10-cm dish). The transfection medium containing Lipo3000 and plasmid mixture was replaced with fresh complete medium after incubation for 4-6 h. Media containing virus was collected 48 h later and clarified by filtration. AML cells were infected with the viruses in the presence of polybrene (5 mg/mL) for 48 h, and then the cells were selected with puromycin.

RNA-seq analysis

For RNA-seq analysis, MV4-11 cells were treated in triplicate with DMSO, 0.1 μM venetoclax, 10 μM HA, or combo (0.1 μM Venetocalx plus 10 μM HA) for 48 h. A total of 12 samples were sequenced using the Illumina NovaSeq 6000 platform. Differentially expressed genes (DEGs) were identified using the DESeq2 package. Genes demonstrating altered expression with a false-discovery rate of $P < 0.01$ and greater than 2-fold change were considered differentially expressed.

QUANTIFICATION AND STATISTICAL ANALYSIS

The results are presented as the mean ± SD. Student's t test was used for comparisons between two groups and one-way analysis of variance was used to compare the means of more than two groups. Survival data were analyzed according to the Kaplan-Meier method by GraphPad Prism 8.0 (GraphPad Software, La Jolla, CA), and P values were determined through the log-rank (Mantel-Cox) test. $P < 0.05$ was considered statistically significant. Data with statistical significance (* $p<0.05$, ** $p<0.01$, *** $p<0.005$, **** $p<0.001$) are shown in Figures.